

ON THE ROTATING NONLINEAR KLEIN-GORDON EQUATION: NON-RELATIVISTIC LIMIT AND NUMERICAL METHODS

NORBERT J. MAUSER, YONG ZHANG, AND XIAOFEI ZHAO

ABSTRACT. We consider numerics / asymptotics for the rotating nonlinear Klein-Gordon (RKG) equation, an important PDE in relativistic quantum physics that can model a rotating galaxy in Minkowski metric and serves also as a model e.g. for a “cosmic superfluid”. Firstly, we formally show that in the non-relativistic limit RKG converges to coupled rotating nonlinear Schrödinger equations (RNLS), which is used to describe the particle-antiparticle pair dynamics. Investigations of the vortex state of RNLS are carried out. Secondly, we propose three different numerical methods to solve RKG from relativistic regimes to non-relativistic regimes in polar and Cartesian coordinates. In relativistic regimes, a semi-implicit finite difference Fourier spectral method is proposed in polar coordinates where both rotation terms are diagonalized simultaneously. While in non-relativistic regimes, to overcome the fast temporal oscillations, we adopt the rotating Lagrangian coordinates and introduce two efficient multiscale methods with uniform accuracy, i.e., the multi-revolution composition method and the exponential integrator. Various numerical results confirm (uniform) accuracy of our methods. Simulations of vortices dynamics are presented.

Keywords: Rotating nonlinear Klein-Gordon equation, cosmological models, non-relativistic limit, rotating two-component BEC, quantized vortex, numerical methods

AMS Subject Classification: 65M06, 65M70, 65Z99, 81Q05, 85A40

1. INTRODUCTION

The universe has been modelled as a “superfluid” since the pioneering work of Witten [67] and Zurek [68]. Such superfluids [44] are often described by a complex-valued scalar field as Ginzburg and Landau proposed an order parameter for the phase coherence [29]. The nonlinear Klein-Gordon equation has then become a popular superfluid model, which is able to cover the entire velocity range, especially the relativistic region [31, 64, 36, 46, 62, 63, 17, 55, 26, 56, 24, 61]. As a model for describing a rotating galaxy in Minkowski metric, the nonlinear Klein-Gordon equation in a rotating frame [31, 36, 46, 62, 63] is used. Also, the nonlinear Klein-Gordon equation appears as a relativistic generalization of the Gross-Pitaevskii equation, a nonlinear Schrödinger equation that serves as a basic model for Bose-Einstein condensates [2], also in the rotating case, see e.g. [2, 69, 58].

From these applications we motivate the following rotating nonlinear Klein-Gordon equation that we study in this work :

$$\frac{1}{c^2} \partial_{tt} \Psi(\mathbf{x}, t) - \Delta \Psi(\mathbf{x}, t) + \left(\frac{mc}{\hbar} \right)^2 \Psi(\mathbf{x}, t) + (V(\mathbf{x}) + m\lambda |\Psi(\mathbf{x}, t)|^2) \Psi(\mathbf{x}, t) - R_{Co} - R_{ce} = 0, \quad (1.1)$$

where the Coriolis term R_{Co} and the centrifugal term R_{ce} read as

$$R_{Co} = i \frac{2\Omega}{c^2} L_z \partial_t \Psi(\mathbf{x}, t), \quad R_{ce} = \frac{\Omega^2}{c^2} L_z^2 \Psi(\mathbf{x}, t), \quad t > 0,$$

and $\mathbf{x} = (x, y) \in \mathbb{R}^2$ or $\mathbf{x} = (x, y, z) \in \mathbb{R}^3$, L_z is the z-component of the angular momentum operator:

$$L_z = -i\hbar(x\partial_y - y\partial_x),$$

$V(\mathbf{x}) : \mathbb{R}^d \rightarrow \mathbb{R}$, $d = 2, 3$ is an external trapping potential and $\Psi = \Psi(\mathbf{x}, t) : \mathbb{R}^d \times \mathbb{R}^+ \rightarrow \mathbb{C}$ is the scalar field. The first order angular momentum operator term R_{Co} describes the Coriolis force and the second order angular term R_{ce} describes the centrifugal force in the rotation. The parameter c is the speed of light, \hbar is the Plank constant, m denotes the mass, λ is the self-interaction constant and Ω denotes the angular velocity.

Equation (1.1) has been used to describe the creation and dynamics of the quantized vortices of a galaxy in 2D or 3D models as a “cosmic rotating superfluid”. The vortices generation that obeys the relativistic Feynman relation, quantum turbulence in the form of a vortex tangle that follows mechanism for matter creation during the big bang era, and the formation and transmission of Kelvin waves correspond well to observations [31, 36, 46, 62, 63]. For generalisations of (1.1) to curved spacetime Klein-Gordon models, e.g. the BTZ metric or the Kerr metric for a black-hole, we refer to [17, 55, 56, 24, 61].

In order to adimensionalize the RKG equation we introduce the scaling

$$\tilde{\mathbf{x}} = \frac{\mathbf{x}}{x_s}, \quad \tilde{t} = \frac{t}{t_s}, \quad \tilde{\Psi}(\tilde{\mathbf{x}}, \tilde{t}) = \Psi(\mathbf{x}, t), \quad t_s = \frac{mx_s^2}{\hbar}, \quad (1.2)$$

where t_s is the time unit and x_s is the length unit, and denote

$$\varepsilon := \frac{\hbar}{mcx_s}, \quad \tilde{\Omega} = \Omega mx_s^2, \quad \tilde{\lambda} = \lambda mx_s^2, \quad \tilde{V}(\tilde{\mathbf{x}}) = x_s^2 V(\mathbf{x}), \quad \tilde{L}_z = -i(\tilde{x}\partial_{\tilde{y}} - \tilde{y}\partial_{\tilde{x}}).$$

Plugging (1.2) into (1.3), the dimensionless rotating nonlinear Klein-Gordon (RKG) equation (removing all the $\tilde{\cdot}$ for simplicity) reads as follows

$$\varepsilon^2 \partial_{tt} \Psi - \Delta \Psi + \frac{1}{\varepsilon^2} \Psi + (V + \lambda |\Psi|^2) \Psi - 2i\Omega \varepsilon^2 L_z \partial_t \Psi - \Omega^2 \varepsilon^2 L_z^2 \Psi = 0, \quad \mathbf{x} \in \mathbb{R}^d, \quad t > 0, \quad (1.3)$$

with $V = V(\mathbf{x})$, $\Psi = \Psi(\mathbf{x}, t)$. The choices of units determine the observation scale of the time evolution of the physical system and decides which phenomena are visible by asymptotic analysis, and which phenomena can be resolved in a numerical discretization by specified spatial/temporal grids. On the RKG, several interesting physical limit regimes can be considered. The dimensionless parameter ε tends to 0 as $\hbar \rightarrow 0$, which is known as the “(semi)classical” limit, or/and as $c \rightarrow \infty$, which is known as the “non-relativistic” or “post-Newtonian” limit. Whereas the semiclassical limit of RKG is largely open (for an overview see [1]), the “non-relativistic limit” of nonlinear KG to Schrödinger type equations is quite well understood, see e.g. [16, 49, 50]. The combined limit from Dirac-Maxwell and KG-Maxwell to Vlasov-Poisson has been given in [52]. The large mass limit of the RKG has been considered in [64].

In this paper, we fix \hbar and consider $\varepsilon \rightarrow 0$ as the non-relativistic limit $c \rightarrow \infty$ and use (1.3) with the usual initial conditions [3, 4, 15, 49, 50, 54, 25]:

$$\Psi(\mathbf{x}, 0) = \psi_0(\mathbf{x}), \quad \partial_t \Psi(\mathbf{x}, 0) = \frac{1}{\varepsilon^2} \psi_1(\mathbf{x}), \quad \mathbf{x} \in \mathbb{R}^d, \quad (1.4)$$

where ψ_0, ψ_1 are complex-valued functions uniformly bounded (with respect to ε) in some Sobolev space. The RKG system (1.3)-(1.4) conserves the (*Hamiltonian*) *energy*

$$E(t) := \int_{\mathbb{R}^d} \left(\varepsilon^2 |\partial_t \Psi|^2 + |\nabla \Psi|^2 + \frac{1}{\varepsilon^2} |\Psi|^2 + V |\Psi|^2 + \frac{\lambda}{2} |\Psi|^4 - \Omega^2 \varepsilon^2 |L_z \Psi|^2 \right) d\mathbf{x} \equiv E(0), \quad t \geq 0, \quad (1.5)$$

and the *charge*

$$Q(t) := \frac{i\varepsilon^2}{2} \int_{\mathbb{R}^d} (\Psi \partial_t \bar{\Psi} - \bar{\Psi} \partial_t \Psi + 2\Omega \Psi (x\partial_y - y\partial_x) \bar{\Psi}) d\mathbf{x}, \quad t \geq 0. \quad (1.6)$$

It is known [13] that the nonlinear Klein-Gordon equation with focusing self-interaction ($\lambda < 0$) can show possible finite time blow-up, whereas for the defocusing case ($\lambda > 0$) existence of the global solution is assured. Our discussion in this work is away from the critical blow-up time.

In this paper, we shall study the dynamics of the RKG (1.3) for a wide range of $\varepsilon \in (0, 1]$ and propose numerical methods for solving (1.3). We shall firstly apply formal analysis to show that the RKG (1.3) converges as $\varepsilon \rightarrow 0$ to a coupled rotating nonlinear Schrödinger equations (RNLS). We discuss the links between the RKG model and the RNLS, where the latter is a classical model for the rotating two-component Bose-Einstein condensates [53, 42, 33, 34, 41]. Quantized vortices lattices will be obtained from the RNLS by minimizing the energy, and we shall then investigate numerically their dynamics in the RKG. In order to efficiently study the dynamics, we propose numerical methods for solving (1.3) in polar or Cartesian coordinates. The polar coordinates are popular for studying vortices dynamics in Schrödinger equation or Ginzburg-Landau equation in

the literature [2, 6, 40, 14, 62, 31, 69, 11]. We shall present a semi-implicit Fourier spectral method in the polar coordinates for the RKG, which simultaneously diagonalizes both rotating terms. In Cartesian coordinates, we aim to overcome the fast temporal oscillation in the solution of (1.3) as $\varepsilon \ll 1$ and simulate efficiently the transition of the RKG in the non-relativistic limit. To do so, we introduce a rotating Lagrangian coordinates transform [8] to (1.3), which helps to eliminate the two rotating terms. Then the state-of-art multiscale methods with uniform discretization accuracy for all $\varepsilon \in (0, 1]$ will be applied for solving (1.3), including the multi-revolution composition method [22] and the exponential integrator [15]. In the end, we apply the presented methods to study the vortices dynamics in the RKG (1.3) for $\varepsilon \in (0, 1]$. Compared to the results in the Schrödinger models [6, 7, 48, 9], relativistic corrections to the vortices dynamics are clearly observed.

The paper is organized as follows. In section 2, we analyze the limit of the RKG as $\varepsilon \rightarrow 0$ and study the limit model. Numerical methods are proposed in section 3. Numerical tests and simulations are reported in section 4. Finally, some conclusions are drawn in section 5. We shall adopt the notation $A \lesssim B$ to represent that there exists a constant $C > 0$ which is independent of ε , such that $|A| \leq CB$.

2. NON-RELATIVISTIC LIMIT

By considering $0 < \varepsilon \ll 1$ in (1.3) in the sense of speed of light c going to infinity, we are in the non-relativistic limit regime of the cosmic rotating superfluid where only quantum effects remain. By formal analysis, we shall show that RKG converges in the limit $\varepsilon \rightarrow 0$ to coupled rotating Gross-Pitevskii type equations describing two-component Bose-Einstein condensates (BEC).

2.1. Formal analysis. Assume that the solution of (1.3) satisfies an expansion [5, 3]:

$$\Psi(\mathbf{x}, t) = e^{it/\varepsilon^2} z_+(\mathbf{x}, t) + e^{-it/\varepsilon^2} \bar{z}_-(\mathbf{x}, t) + r(\mathbf{x}, t), \quad \mathbf{x} \in \mathbb{R}^d, \quad t \geq 0, \quad (2.1)$$

where $z_{\pm} = z_{\pm}(\mathbf{x}, t)$ and $r = r(\mathbf{x}, t)$ are unknowns to be determined. Note that the fast oscillating phase factors correspond to the rest energy, like in the Foldy-Wouthouse transform for the non-relativistic limit of the Dirac equation (see e.g. [51]). Plugging (2.1) into the equation (1.3), we get

$$\begin{aligned} & e^{is/\varepsilon^2} [2i\partial_t - \Delta + V + \lambda(|z_+|^2 + 2|z_-|^2) + 2\Omega L_z] z_+ \\ & + e^{-is/\varepsilon^2} [-2i\partial_t - \Delta + V + \lambda(|z_-|^2 + 2|z_+|^2) - 2\Omega L_z] \bar{z}_- \\ & + \varepsilon^2 \partial_{tt} r - \Delta r + \frac{r}{\varepsilon^2} + e^{3it/\varepsilon^2} z_+^2 z_- + e^{-3it/\varepsilon^2} \bar{z}_-^2 \bar{z}_+ + \varepsilon^2 f_+ + \varepsilon^2 f_- + f_r = 0, \end{aligned}$$

where

$$\begin{aligned} f_+ &= e^{it/\varepsilon^2} (\partial_{tt} - 2i\Omega L_z \partial_t - \Omega^2 L_z^2) z_+, \quad f_- = e^{-it/\varepsilon^2} (\partial_{tt} - 2i\Omega L_z \partial_t - \Omega^2 L_z^2) \bar{z}_-, \\ f_r &= e^{it/\varepsilon^2} \lambda (2z_+ |r|^2 + z_- r^2) + e^{-it/\varepsilon^2} \lambda (2\bar{z}_- |r|^2 + \bar{z}_+ r^2) + e^{2it/\varepsilon^2} \lambda (z_+^2 \bar{r} + 2z_+ z_- r) \\ & + e^{-2it/\varepsilon^2} \lambda (\bar{z}_-^2 \bar{r} + 2\bar{z}_+ \bar{z}_- r) + 2\lambda (z_+ \bar{z}_- \bar{r} + |z_+|^2 r + |z_-|^2 r + |r|^2 r) + Vr. \end{aligned}$$

We can decompose the RKG equation into a pair of coupled Schrödinger equations:

$$\begin{cases} 2i\partial_t z_+ - \Delta z_+ + V z_+ + \lambda(|z_+|^2 + 2|z_-|^2) z_+ + 2\Omega L_z z_+ = 0, \\ 2i\partial_t z_- - \Delta z_- + V z_- + \lambda(|z_-|^2 + 2|z_+|^2) z_- + 2\Omega L_z z_- = 0, \end{cases} \quad (2.2)$$

and an equation for the remainder :

$$\varepsilon^2 \partial_{tt} r - \Delta r + \frac{r}{\varepsilon^2} + e^{3it/\varepsilon^2} z_+^2 z_- + e^{-3it/\varepsilon^2} \bar{z}_-^2 \bar{z}_+ + \varepsilon^2 f_+ + \varepsilon^2 f_- + f_r = 0. \quad (2.3)$$

Based on the ansatz (2.1) and the initial condition (1.4), we have at $t = 0$

$$\begin{cases} z_+(\mathbf{x}, 0) + \bar{z}_-(\mathbf{x}, 0) + r(\mathbf{x}, 0) = \psi_0(\mathbf{x}), \\ \frac{i}{\varepsilon^2} [z_+(\mathbf{x}, 0) - \bar{z}_-(\mathbf{x}, 0)] + \partial_t z_+(\mathbf{x}, 0) + \partial_t \bar{z}_-(\mathbf{x}, 0) + \partial_t r(\mathbf{x}, 0) = \frac{\psi_1(\mathbf{x})}{\varepsilon^2}. \end{cases}$$

If we consider (2.2) associated with initial values

$$z_+(\mathbf{x}, 0) = \frac{1}{2}(\psi_0(\mathbf{x}) - i\psi_1(\mathbf{x})), \quad z_-(\mathbf{x}, 0) = \frac{1}{2}(\overline{\psi_0(\mathbf{x})} - i\overline{\psi_1(\mathbf{x})}), \quad (2.4)$$

it leaves

$$r(\mathbf{x}, 0) = 0, \quad \partial_t r(\mathbf{x}, 0) = -\partial_t z_+(\mathbf{x}, 0) - \partial_t \overline{z_-(\mathbf{x}, 0)}.$$

When $\varepsilon \rightarrow 0$, the RKG (1.3) converges to the two coupled nonlinear Schrödinger equations with angular momentum rotation (2.2) and initial values (2.4), which is guaranteed by the following estimate:

Lemma 2.1. *Under the regularity assumption $\psi_0(\mathbf{x}), \psi_1(\mathbf{x}), V(\mathbf{x}) \in H^{m_0+4}(\mathbb{R}^d)$, $m_0 > d/2$, we have*

$$\|r(\cdot, t)\|_{H^{m_0}} \lesssim \varepsilon^2, \quad 0 \leq t \leq T, \quad (2.5)$$

for some $T > 0$ independent of ε .

Proof. Based on the assumption, we have directly $z_{\pm}(\mathbf{x}, 0) \in H^{m_0+4}(\mathbb{R}^d)$. Note $L_z = -i\partial_\theta$ and denote $\mathcal{L} = -\Delta - 2i\Omega\partial_\theta$. Then for the Schrödinger system (2.7), we have

$$z_{\pm}(\mathbf{x}, t) = e^{it/2\mathcal{L}} z_{\pm}(\mathbf{x}, 0) + \frac{i}{2} \int_0^t e^{i(t-s)/2\mathcal{L}} [V(\mathbf{x}) + \lambda(|z_{\pm}(\mathbf{x}, s)|^2 + 2|z_{\mp}(\mathbf{x}, s)|^2)] z_{\pm}(\mathbf{x}, s) ds.$$

Since $e^{it/2\mathcal{L}}$ is bounded, then by the formal bootstrap argument, we have

$$\partial_t^k z_{\pm}(\mathbf{x}, t) \in L^\infty((0, T); H^{m_0+4-2k}(\mathbb{R}^d)), \quad k = 0, 1, 2,$$

for some $T > 0$. It is then straightforward to see

$$f_{\pm}(\mathbf{x}, t) \in L^\infty((0, T); H^{m_0}(\mathbb{R}^d)).$$

For the remainder's equation:

$$\begin{cases} \varepsilon^2 \partial_{tt} r - \Delta r + \frac{r}{\varepsilon^2} + e^{3it/\varepsilon^2} z_+^2 z_- + e^{-3it/\varepsilon^2} \overline{z_-^2 z_+} + \varepsilon^2 f_+ + \varepsilon^2 f_- + f_r = 0, \\ r(\mathbf{x}, 0) = 0, \quad \partial_t r(\mathbf{x}, 0) = -\partial_t z_+(\mathbf{x}, 0) - \partial_t z_-(\mathbf{x}, 0), \end{cases}$$

we have by Duhamel's formula in Fourier space,

$$\begin{aligned} \widehat{r}(\xi, t) &= \frac{\sin(\omega_\xi t)}{\omega_\xi} \widehat{(\partial_t r)}(\xi, 0) - \int_0^t \frac{\sin(\omega_\xi(t-\theta))}{\varepsilon^2 \omega_\xi} \left[\varepsilon^2 \widehat{f_+}(\xi, \theta) + \varepsilon^2 \widehat{f_-}(\xi, \theta) + \widehat{f_r}(\xi, \theta) \right] d\theta \\ &\quad - \int_0^t \frac{\sin(\omega_\xi(t-\theta))}{\varepsilon^2 \omega_\xi} \left[e^{3i\theta/\varepsilon^2} \widehat{(z_+^2 z_-)}(\xi, \theta) + e^{-3i\theta/\varepsilon^2} \widehat{(z_-^2 z_+)}(\xi, \theta) \right] d\theta, \quad \xi \in \mathbb{R}^d, \end{aligned} \quad (2.6)$$

with $\omega_\xi = \frac{1}{\varepsilon^2} \sqrt{1 + \varepsilon^2 |\xi|^2}$. Defining

$$\int_0^t \frac{\sin(\omega_\xi(t-\theta))}{\varepsilon^2 \omega_\xi} e^{3i\theta/\varepsilon^2} d\theta = \frac{\varepsilon^2 \omega_\xi (e^{3it/\varepsilon^2} - \cos(\omega_\xi t)) - 3i \sin(\omega_\xi t)}{\omega_\xi (\varepsilon^4 \omega_\xi^2 - 9)} =: \varphi(\xi, t),$$

we have

$$\varphi(\xi) = O(\varepsilon^2), \quad |\xi| \leq 2\varepsilon^{-1}.$$

Therefore in (2.6) for $|\xi| \leq 2\varepsilon^{-1}$, we use an integration-by-parts argument to write, e.g. (same to the rests)

$$\begin{aligned} \int_0^t \frac{\sin(\omega_\xi(t-\theta))}{\varepsilon^2 \omega_\xi} e^{3i\theta/\varepsilon^2} \widehat{(z_+^2 z_-)}(\xi, \theta) d\theta &= \varphi(\xi, t) \widehat{(z_+^2 z_-)}(\xi, t) - \varphi(\xi, 0) \widehat{(z_+^2 z_-)}(\xi, 0) \\ &\quad - \int_0^t \varphi(\xi, \theta) (\partial_t \widehat{(z_+^2 z_-)})(\xi, \theta) d\theta, \quad |\xi| \leq 2\varepsilon^{-1}. \end{aligned}$$

With the Parserval's identity, we get from (2.6) for $0 \leq t \leq T$,

$$\begin{aligned} & \|r(\cdot, t)\|_{H^{m_0}} \\ & \lesssim \varepsilon^2 \|\partial_t r(\cdot, 0)\|_{H^{m_0}} + \int_0^t \varepsilon^2 (\|f_+(\cdot, \theta)\|_{H^{m_0}} + \|f_-(\cdot, \theta)\|_{H^{m_0}}) d\theta + \int_0^t \|f_r(\cdot, \theta)\|_{H^{m_0}} d\theta \\ & + \varepsilon^2 (1+t) (\|z_+\|_{L^\infty((0,T);H^{m_0})} + \|\partial_t z_+\|_{L^\infty((0,T);H^{m_0})} + \|z_-\|_{L^\infty((0,T);H^{m_0})} + \|\partial_t z_-\|_{L^\infty((0,T);H^{m_0})}) \\ & + \int_0^t (\|z_+^2 z_-(\cdot, \theta) - P_\varepsilon(z_+^2 z_-)(\cdot, \theta)\|_{H^{m_0}} + \|z_-^2 z_+(\cdot, \theta) - P_\varepsilon(z_-^2 z_+)(\cdot, \theta)\|_{H^{m_0}}) d\theta, \end{aligned}$$

with P_ε the projection operator

$$P_\varepsilon f(\mathbf{x}, t) := \int_{|\xi| \leq 2\varepsilon^{-1}} \widehat{f}(\xi, t) e^{2\pi i \mathbf{x} \cdot \xi} d\xi.$$

It is clear to have

$$\|z_+^2 z_-(\cdot, t) - P_\varepsilon(z_+^2 z_-)(\cdot, t)\|_{H^{m_0}} \lesssim \varepsilon^2 \|z_+^2 z_-(\cdot, t)\|_{H^{m_0+2}} \lesssim \varepsilon^2.$$

So we get

$$\|r(\cdot, t)\|_{H^{m_0}} \lesssim \varepsilon^2 + \int_0^t \|f_r(\cdot, \theta)\|_{H^{m_0}} d\theta, \quad 0 \leq t \leq T.$$

Noting that $f_r = O(r)$, we get by using the bootstrap argument

$$\|r(\cdot, t)\|_{H^{m_0}} \lesssim \varepsilon^2, \quad 0 < t \leq T',$$

for some $0 < T' \leq T$ independent of ε . \square

2.2. The limit system. As shown in Lemma 2.1, the limit system of the RKG when $\varepsilon \rightarrow 0$ is the rotating coupled nonlinear Schrödinger equation (RNLS) given below

$$\begin{cases} 2i\partial_t z_+ - \Delta z_+ + Vz_+ + \lambda(|z_+|^2 + 2|z_-|^2)z_+ + 2\Omega L_z z_+ = 0, & \mathbf{x} \in \mathbb{R}^d, t > 0, \\ 2i\partial_t z_- - \Delta z_- + Vz_- + \lambda(|z_-|^2 + 2|z_+|^2)z_- + 2\Omega L_z z_- = 0, \\ z_+(\mathbf{x}, 0) = \frac{1}{2}(\psi_0(\mathbf{x}) - i\psi_1(\mathbf{x})), \quad z_-(\mathbf{x}, 0) = \frac{1}{2}(\overline{\psi_0}(\mathbf{x}) - i\overline{\psi_1}(\mathbf{x})). \end{cases} \quad (2.7)$$

We shall briefly discuss this limit model in the following, mainly to link with the research work on RNLS in the literature and to compare with the RKG.

As a matter of fact, the limit system RNLS reads similarly as the models for the rotating two-component Bose-Einstein condensates (BEC), which have received wide attentions in the literature [53, 42, 33, 34, 41, 48, 58]. Lemma 2.1 gives a formal justification from the rotating Klein-Gordon model for cosmic superfluid to the rotating two-component BEC model through the non-relativistic limit, and rigorous mathematical analysis could also be done by following the way in [49, 50, 54]. Here in our decomposition (2.1), according to the Dirac's hole theory or quantum field theory, z_+ represents (*normal*) *particles* with positive charge and z_- represents *antiparticles* with negative charge [19, 66]. Same as for BEC, the RNLS (2.7) conserves the *mass* or the L^2 -norm of each component

$$M_\pm(t) := \int_{\mathbb{R}^d} |z_\pm|^2 d\mathbf{x} \equiv M_\pm(0), \quad t \geq 0, \quad (2.8)$$

and the (*Hamiltonian*) *energy*

$$\begin{aligned} E_{nls}(t) & := \frac{1}{2} \int_{\mathbb{R}^2} \left(|\nabla z_+|^2 + |\nabla z_-|^2 + V|z_+|^2 + V|z_-|^2 + \frac{\lambda}{2} (|z_+|^4 + |z_-|^4 + 2|z_+|^2|z_-|^2) \right) d\mathbf{x} \\ & - \Omega \int_{\mathbb{R}^d} \operatorname{Re}(\overline{z_+} L_z z_+ + \overline{z_-} L_z z_-) d\mathbf{x} \equiv E_{nls}(0), \quad t \geq 0. \end{aligned} \quad (2.9)$$

The gap between RKG and RNLS is $O(\varepsilon^2)$ by result (2.5). The charge conservation law (1.6) of RKG transits to mass conservation of RNLS through the limit $\varepsilon \rightarrow 0$. In fact, by plugging the

expansion (2.1) into the charge (1.6), we have

$$Q(t) = \int_{\mathbb{R}^d} (|z_+|^2 - |z_-|^2) d\mathbf{x} + O(\varepsilon^2).$$

The mass conservations (2.8) imply that $\|z_+\|_{L^2}^2 - \|z_-\|_{L^2}^2$ is a time-independent quantity which acts as the leading order approximation of the charge Q in the non-relativistic limit. Moreover, compared with RKG, RNLS in general contains only the Coriolis force term, i.e. $L_z z_{\pm}$. The centrifugal force term R_{ce} in RKG, however, is a higher order perturbation in the non-relativistic limit regime, and it vanishes as $\varepsilon \rightarrow 0$. Therefore, we say that the **RKG is more comprehensive**, and by considering a wide range of $\varepsilon \in (0, 1]$, one would expect to observe more interesting phenomena in RKG than in RNLS. The detailed relations between the two models are summarized in Tab. 1.

TABLE 1. Non-relativistic limit of the rotating Klein-Gordon equation.

$\varepsilon \rightarrow 0$	Rotating cosmic superfluid	Rotating two-component BEC
Model	Rotating nonlinear KG equation	Rotating coupled NLS equations
Angular term	Centrifugal term&Coriolis term	Coriolis term
Charge	Conserve charge (1.6)	Conserve Mass (2.8)
Energy	Conserve Hamiltonian (1.5)	Conserve Hamiltonian (2.9)

Thanks to the model gap $O(\varepsilon^2)$, the limit model (2.7) serves as a valid approximation to the original problem in the regime $0 < \varepsilon \ll 1$, which is a popular option in the literature to study multiscale systems [21, 27]. However, this general theoretical estimate $O(\varepsilon^2)$ could never prescribe the precise regime of ε that the RNLS model is qualitatively correct for a particular physical phenomenon. By tuning the ε in RKG, we are going to investigate the validity of RNLS in studying the dynamics of quantized vortices states of RNLS in RKG later. The quantized vortices states are of great interests and importance in both BEC [2, 48, 42] and cosmic superfluid [30, 37, 62, 31]. The vortices states of RNLS can be obtained by considering the ground state.

The ground state of RNLS (2.7) can be defined as the minimizer of the energy functional (2.9) under constraints: $M_{\pm} = 1$. For (2.7), we have the same existence result of the ground state as the classical rotating BEC [2]: when the trapping potential is chosen as a harmonic function, i.e. $V = \frac{1}{2}(\gamma_x^2 x^2 + \gamma_y^2 y^2)$ with $\gamma_x > 0, \gamma_y > 0$ being the trapping frequency in x, y direction respectively, then the ground state of (2.7) exists if $|\Omega| < \Omega_c$ and $\lambda > -\lambda_c$, for some critical values $\Omega_c, \lambda_c > 0$. We refer the readers to [2] for more details. The ground state under fast rotating speed contains quantized vortices. However, it remains problematic in computing the ground state of two-component BEC due to the lack of numerical techniques, which will be addressed in a coming work. Here, we adopt the normalized gradient flow method [2]. It is clear that if one starts the gradient flow of the Hamiltonian E_{nls} from two identical states for the two components z_{\pm} , then in the ground state found by the algorithm, the two components would also be completely the same. To avoid this case, here we apply the normalized gradient flow to minimize the Hamiltonian starting from two different states:

$$z_+^0 = \frac{(1 - \Omega)\phi_g(x, y) + \Omega\phi_g(x, y)(x - iy)}{\|(1 - \Omega)\phi_g(x, y) + \Omega\phi_g(x, y)(x - iy)\|}, \quad z_-^0 = \overline{z_+^0},$$

where $\phi_g(x, y) := e^{-\frac{x^2+y^2}{2}}/\sqrt{\pi}$. We remark that this strategy will lead to a general bound state which is not necessarily a ground state.

Fig. 1 shows the bound state $z_+(\mathbf{x}), z_-(\mathbf{x})$ under $\lambda = 50, V = \frac{1}{2}(x^2 + y^2)$ and $\Omega = 0.9$ found by the normalized gradient flow and the quantization $z_+(\mathbf{x}) + \overline{z_-(\mathbf{x})}$. In quantum field theory,

$$e^{i\gamma} z_+ + e^{-i\gamma} \overline{z_-}, \quad \gamma \in \mathbb{R},$$

gives the quantization of the field. We shall use this bound state of the RNLS to produce a vortices pattern and later study its dynamics in the RKG for some $0 < \varepsilon \leq 1$. When $0 < \varepsilon \ll 1$, the vortices pattern in RKG should dynamically remain like a steady state with only rotation. By

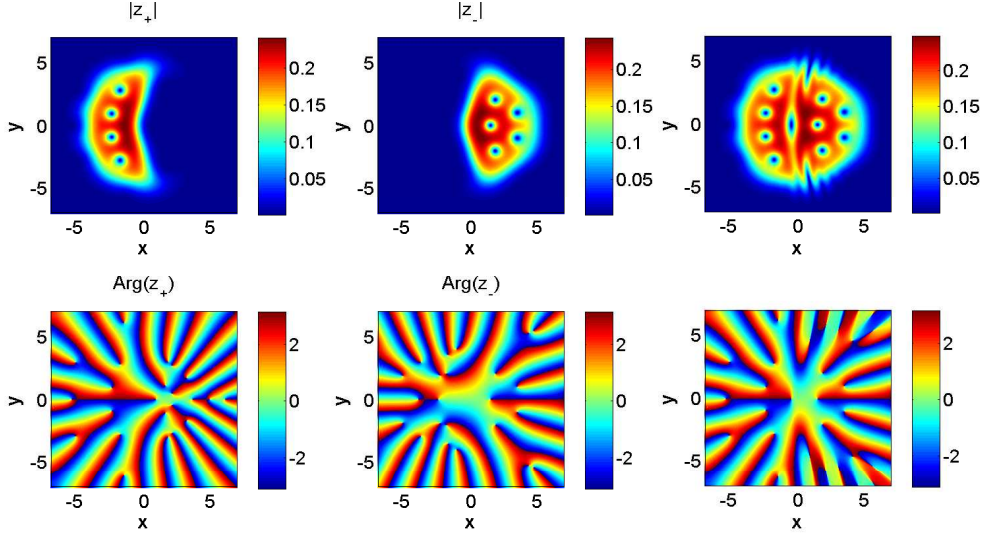


FIGURE 1. Contour plot of the bound state of the particle $z_+(\mathbf{x})$ (left), antiparticle $z_-(\mathbf{x})$ (middle) and the quantization $z_+(\mathbf{x}) + \bar{z}_-(\mathbf{x})$ (right) for $\omega = 0.9$.

tuning the $\varepsilon \in (0, 1]$ in the RKG model, we are able to cover the relativistic regime and non-relativistic regime. In fact, the BEC models have already been considered for studying cosmology in the physics without considering the relativistic effect, see e.g. [39] and the references therein. Hence, through our study in vortices dynamics in RKG under different ε , we are also expected to observe the relativistic correction to BEC. That motivates us to consider a robust numerical solver for RKG for all $\varepsilon \in (0, 1]$.

Remark 2.2. One can apply formal derivation and analysis to the rotating Klein-Gordon equation with more general power-law nonlinearity or higher order term. The resulting limit system would be modified with the corresponding generalized nonlinear terms.

3. NUMERICAL METHODS

In this section, we propose numerical methods for computing the dynamics of RKG (1.3). We shall present efficient and accurate discretizations in polar coordinates and in the rotating Lagrangian coordinates in a sequel. The method in the polar coordinates works well for RKG with $\varepsilon \approx 1$, while in the rotating Lagrangian coordinates, two uniformly accurate methods for all $\varepsilon \in (0, 1]$ will be introduced. For simplicity, we illustrate numerical methods in 2D.

3.1. Polar Coordinates. It has been popular to simulate the quantized vortices dynamics on a disk-shaped domain in polar coordinates [2, 6, 14, 62, 31, 69, 40, 11], where the angular momentum operator reads simply as derivative with respect to the angle, i.e. $L_z = -i\partial_\theta$. In fact, the numerical scheme in polar coordinates has been called in [62] to study the vortices dynamics under relativistic Feynman relation in RKG. Here we present such scheme in details. To do so, it is convenient to truncate the whole space problem onto a disk

$$\Omega_{R_0} := \{\mathbf{x} \in \mathbb{R}^2 \mid |\mathbf{x}| \leq R_0\},$$

and to impose homogenous Neumann boundary condition, where the radius $R_0 > 0$ is large enough to hold the dynamics. In polar coordinates, (1.3) reads as follows

$$\varepsilon^2 (\partial_{tt} - 2\Omega\partial_{t\theta} + \Omega^2\partial_{\theta\theta}) \Psi - \left(\partial_{rr} + \frac{1}{r}\partial_r + \frac{1}{r^2}\partial_{\theta\theta} \right) \Psi + \frac{1}{\varepsilon^2} \Psi + (V + \lambda|\Psi|^2) \Psi = 0, \quad (3.1)$$

with initial values and boundary conditions

$$\begin{aligned}\Psi(r, \theta, t = 0) &= \psi_0(r, \theta), \quad \partial_t \Psi(r, \theta, t = 0) = \frac{1}{\varepsilon^2} \psi_1(r, \theta), \quad 0 \leq r \leq R_0, \quad 0 \leq \theta \leq 2\pi, \\ \partial_r \Psi(R_0, \theta, t) &= 0, \quad |\Psi(0, \theta, t)| < \infty, \quad t \geq 0, \quad 0 \leq \theta \leq 2\pi, \\ \Psi(r, 0, t) &= \Psi(r, 2\pi, t), \quad \partial_\theta \Psi(r, 0, t) = \partial_\theta \Psi(r, 2\pi, t), \quad t \geq 0, \quad 0 \leq r \leq R_0.\end{aligned}$$

Semi-implicit finite difference Fourier spectral method. We present a semi-implicit (also known as IMEX) finite difference Fourier spectral (**SIFS**) method to solve (3.1). Firstly, thanks to the periodicity in θ , we approximate the wave function Ψ by a truncated Fourier series, i.e.

$$\Psi(r, \theta) \approx \sum_{k=-N_\theta/2}^{N_\theta/2-1} \widehat{\Psi}_k(r) e^{ik\theta}, \quad \theta \in [0, 2\pi], \quad (3.2)$$

with N_θ being an even integer. The Fourier coefficient $\widehat{\Psi}_k(r)$ is defined and approximated as

$$\widehat{\Psi}_k(r) = \frac{1}{2\pi} \int_0^{2\pi} \Psi(r, \theta) e^{-ik\theta} d\theta \approx \frac{1}{N_\theta} \sum_{j=0}^{N_\theta-1} \Psi(r, j\Delta\theta) e^{-ikj\Delta\theta},$$

with $\Delta\theta = \frac{2\pi}{N_\theta}$. Plugging (3.2) into (3.1), we have for $k = -N_\theta/2, \dots, N_\theta/2 - 1$,

$$\varepsilon^2 (\partial_{tt} - 2\Omega ik \partial_t - \Omega^2 k^2) \widehat{\Psi}_k = \left(\partial_{rr} + \frac{1}{r} \partial_r - \frac{k^2}{r^2} \right) \widehat{\Psi}_k - \frac{1}{\varepsilon^2} \widehat{\Psi}_k + (\widehat{F(\Psi)})_k, \quad 0 \leq r < R_0, \quad (3.3)$$

with $F(\Psi) = -(V + \lambda|\Psi|^2)\Psi$. Notice that all θ -derivatives terms are diagonalized explicitly. However, diagonalising the operators in r -direction is not so simple. One may consider to use the Laguerre polynomials as basis [7], but then there are no fast transform algorithms. Consequently, the state-of-the-art time integrators [35, 32] and multiscale techniques [3, 15, 22] which evaluate the stiff linear part exactly *can not* be applied in an efficient way. Hence, to evolve (3.3) from time $t_n := n\Delta t$ to t_{n+1} by a time step $\Delta t > 0$, it is more convenient to apply a classical three-level semi-implicit finite difference scheme as follows

$$\varepsilon^2 (\delta_t^2 - 2\Omega ik \delta_t - \Omega^2 k^2 \mu_t) \widehat{\Psi}_k^n = \left(\partial_{rr} + \frac{1}{r} \partial_r - \frac{k^2}{r^2} - \frac{1}{\varepsilon^2} \right) (\widehat{\mu_t \Psi^n})_k + (\widehat{F(\Psi^n)})_k, \quad n \geq 1, \quad (3.4)$$

where Ψ^n is the numerical approximation of $\Psi(\cdot, t_n)$, and

$$\delta_t \Psi^n = \frac{\Psi^{n+1} - \Psi^{n-1}}{2\Delta t}, \quad \delta_t^2 \Psi^n = \frac{\Psi^{n+1} - 2\Psi^n + \Psi^{n-1}}{(\Delta t)^2}, \quad \mu_t \Psi^n = \frac{1}{2}(\Psi^{n+1} + \Psi^{n-1}).$$

Equation (3.4) is numerically further discretized in r -direction by a second order finite difference method on a uniform mesh with a half-grid shift [45, 47]. We choose integer $N_r > 0$ and denote $r_j = (j - 1/2)\Delta r$ with $\Delta r = R_0/N_r, j = 0, 1, \dots, N_r + 1$. The full discretization then reads:

$$\varepsilon^2 (\delta_t^2 - 2\Omega ik \delta_t) \widehat{\Psi}_{k,j}^n = \left(\Delta_r - \frac{1}{\varepsilon^2} + \varepsilon^2 \Omega^2 k^2 \right) (\widehat{\mu_t \Psi^n})_{k,j} + (\widehat{F(\Psi^n)})_{k,j}, \quad n \geq 1, \quad (3.5)$$

for $k = -N_\theta/2, \dots, N_\theta/2 - 1, j = 1, \dots, N_r$. Here we define the discrete operator $\Delta_r \widehat{\Psi}_{k,j}^n$ as follows:

$$\Delta_r \widehat{\Psi}_{k,j}^n = \frac{\widehat{\Psi}_{k,j+1}^n - 2\widehat{\Psi}_{k,j}^n + \widehat{\Psi}_{k,j-1}^n}{(\Delta r)^2} + \frac{1}{r_j} \frac{\widehat{\Psi}_{k,j+1}^n - \widehat{\Psi}_{k,j-1}^n}{2\Delta r} - \frac{k^2}{r_j^2} \widehat{\Psi}_{k,j}^n, \quad j = 1, \dots, N_r, \quad (3.6)$$

where $\widehat{\Psi}_{k,j}^n$ is an approximation of $\widehat{\Psi}_k^n(r_j)$. For the boundary values, i.e. $j = N_r + 1$, the homogeneous Neumann boundary condition implies $\widehat{\Psi}_{k,N_r}^n = \widehat{\Psi}_{k,N_r+1}^n, \forall n \in \mathbb{N}$. Using the half-grid shift grids, we *do not* have to deal with the singularity at $r = 0$ or imposing any boundary conditions thereof [45, 47]. To complete the scheme, the starting values can be obtained explicitly as $\Psi^0 = \psi_0$ and

$$\begin{aligned}\Psi^1 &= \Psi^0 + \Delta t \partial_t \Psi(\cdot, t = 0) + \frac{(\Delta t)^2}{2} \partial_{tt} \Psi(\cdot, t = 0) \\ &= \Psi^0 + \Delta t \frac{1}{\varepsilon^2} \psi_1 + \frac{(\Delta t)^2}{2} \partial_{tt} \Psi(\cdot, t = 0),\end{aligned} \quad (3.7)$$

where $\partial_{tt}\Psi(\cdot, t=0)$ can be obtained explicitly by setting $t=0$ in (3.1).

The SIFS scheme is semi-implicit, however, at each time level, it only requires a tri-diagonal linear solver, and it is quite simple with Thomas algorithm and cheap with $O(N_r N_\theta \log N_\theta)$ complexity. The semi-implicit treatment makes the scheme free with CFL conditions [4], but it could be unstable in practice when ε becomes small [43]. Moreover, the finite difference integrator has under-resolution as ε turns to zero. This can be seen by the error bound. Since the solution $\Psi(\mathbf{x}, t)$ propagates waves with wavelength $O(\varepsilon^2)$ in time which implies $\partial_{ttt}\Psi = O(\varepsilon^{-6})$, the error bound of SIFS up to a fixed time is

$$O\left(\frac{\Delta t^2}{\varepsilon^6}\right) + O(\Delta r^2) + O(\Delta\theta^{m_0}),$$

with some $m_0 > 0$ depends on the regularity of the solution in θ . Therefore, to obtain a correct approximation, one needs to adopt $\Delta t = O(\varepsilon^3)$, which brings heavy computational burden for $0 < \varepsilon \ll 1$ in the non-relativistic limit regime. By the above and the numerical evidence as we shall see later, SIFS is a proper solve for RKG on a disk domain in the relativistic regime, i.e. $\varepsilon \approx 1$, though it becomes problematic for small ε and this motivates us to seek for other techniques.

Remark 3.1. Alternative to the finite difference method in SIFS for the radius discretization, the Chebyshev spectral method [59, 18, 57] can be applied for discretizing (3.4) in r direction. We choose the Chebyshev collocation method in r direction with Gauss-Chebyshev-Radau points $r_j := \frac{R_0}{2}(1 - x_j) = \frac{R_0}{2}(1 + \cos(\frac{2\pi(N_r-j)}{2N_r+1}))$, $j = 0, 1, \dots, N_r$, $r_{N_r} = R_0$. For the sake of brevity here, we refer the readers to [57, 59] for more details of the implementation. In combined with the same semi-implicit finite difference integrator and Fourier spectral method in θ direction, it improves the total error to $O(\Delta t^2/\varepsilon^6) + O(\Delta r^{m_1}) + O(\Delta\theta^{m_0})$ with some $m_1 > 0$ depends on the regularity of the solution in r . When the solution is smooth in r , one gets spectral accuracy in spatial discretization.

3.2. Rotating Lagrangian coordinates. To propose an efficient algorithm for solving (1.3) for a wide range of $\varepsilon \in (0, 1]$, we need to overcome the fast temporal oscillation of the solution in the non-relativistic limit by some multiscale integration methods. However, the Coriolis rotating term $2i\Omega\varepsilon^2 L_z \partial_t \Psi$ and the centrifugal force term $\Omega^2 \varepsilon^2 L_z^2 \Psi$ in the RKG equation prevents applications of the popular multiscale strategies like in [3, 20, 22, 15] to (1.3). Here, borrowing the idea of coordinates transform from the rotating BEC [48, 8], we introduce the rotating Lagrangian coordinates and perform a coordinates transform to (1.3).

We introduce the rotating matrix

$$A(t) := \begin{pmatrix} \cos(\Omega t) & \sin(\Omega t) \\ -\sin(\Omega t) & \cos(\Omega t) \end{pmatrix}, \quad t \geq 0,$$

and denote the unknown of the RKG (1.3) in the *rotating Lagrangian coordinates* as:

$$u(\tilde{\mathbf{x}}, t) = \Psi(\mathbf{x}, t), \quad \mathbf{x} = A(t)\tilde{\mathbf{x}}. \quad (3.8)$$

Directly we have

$$\begin{aligned} \partial_t u &= \nabla \Psi(\dot{A}\tilde{\mathbf{x}}) + \partial_t \Psi, \\ \partial_{tt} u &= (\dot{A}\tilde{\mathbf{x}})^T \nabla^2 \Psi(\dot{A}\tilde{\mathbf{x}}) + \nabla \Psi(\ddot{A}\tilde{\mathbf{x}}) + 2\nabla \partial_t \Psi(\dot{A}\tilde{\mathbf{x}}) + \partial_{tt} \Psi. \end{aligned} \quad (3.9)$$

Noting that

$$\dot{A}\tilde{\mathbf{x}} = \Omega \begin{pmatrix} y \\ -x \end{pmatrix}, \quad \ddot{A}\tilde{\mathbf{x}} = -\Omega^2 \mathbf{x}, \quad (\dot{A}\tilde{\mathbf{x}})^T \nabla^2 \Psi(\dot{A}\tilde{\mathbf{x}}) = \Omega^2 (x^2 \partial_{yy} \Psi - 2xy \partial_{xy} \Psi + y^2 \partial_{xx} \Psi),$$

(3.9) becomes

$$\partial_{tt} u = \Omega^2 (x^2 \partial_{yy} \Psi - 2xy \partial_{xy} \Psi + y^2 \partial_{xx} \Psi - x \partial_x \Psi - y \partial_y \Psi) + 2\Omega (y \partial_{xt} \Psi - x \partial_{yt} \Psi) + \partial_{tt} \Psi.$$

Using the facts:

$$L_z \partial_t \Psi = i(y \partial_{xt} \Psi - x \partial_{yt} \Psi), \quad L_z^2 \Psi = -x^2 \partial_{yy} \Psi + 2xy \partial_{xy} \Psi - y^2 \partial_{xx} \Psi + x \partial_x \Psi + y \partial_y \Psi,$$

we see

$$\partial_{tt} u = -\Omega^2 L_z^2 \Psi - 2i\Omega L_z \partial_t \Psi + \partial_{tt} \Psi.$$

By further noting that

$$\Delta_{\tilde{\mathbf{x}}}u = \Delta\Psi,$$

we get the *RKG in the rotating Lagrangian coordinates*:

$$\varepsilon^2 \partial_{tt}u(\tilde{\mathbf{x}}, t) - \Delta u(\tilde{\mathbf{x}}, t) + \frac{1}{\varepsilon^2}u(\tilde{\mathbf{x}}, t) + [V(A(t)\tilde{\mathbf{x}}) + \lambda|u(\tilde{\mathbf{x}}, t)|^2] u(\tilde{\mathbf{x}}, t) = 0, \quad \tilde{\mathbf{x}} \in \mathbb{R}^2, \quad t > 0, \quad (3.10a)$$

$$u(\tilde{\mathbf{x}}, 0) = \psi_0(\tilde{\mathbf{x}}), \quad \partial_t u(\tilde{\mathbf{x}}, 0) = \Omega \nabla \psi_0(\tilde{\mathbf{x}}) \begin{pmatrix} \tilde{y} \\ -\tilde{x} \end{pmatrix} + \frac{1}{\varepsilon^2} \psi_1(\tilde{\mathbf{x}}), \quad \tilde{\mathbf{x}} \in \mathbb{R}^2, \quad (3.10b)$$

where the angular momentum terms have been eliminated and (3.10) is simply a nonlinear Klein-Gordon equation. When the trapping potential $V(\mathbf{x})$ is isotropic, i.e. $V(\mathbf{x}) = U(|\mathbf{x}|)$ for some function $U(\cdot) : \mathbb{R} \rightarrow \mathbb{R}$, then $V(A(t)\tilde{\mathbf{x}}) = V(\tilde{\mathbf{x}})$ in (3.10), and the RKG in the rotating frame (3.10) is also an Hamiltonian system without external time dependence. We shall remove all the $\tilde{\cdot}$ in (3.10) in the following for simplicity.

For the numerical discretization, we truncate the whole space problem (3.10) onto a bounded interval $I = (-a, a) \times (b, b) \in \mathbb{R}^2$ and impose approximately the periodic boundary conditions:

$$\varepsilon^2 \partial_{tt}u(\mathbf{x}, t) - \Delta u(\mathbf{x}, t) + \frac{1}{\varepsilon^2}u(\mathbf{x}, t) + [V(A(t)\mathbf{x}) + \lambda|u(\mathbf{x}, t)|^2] u(\mathbf{x}, t) = 0, \quad \mathbf{x} \in I, \quad t > 0, \quad (3.11a)$$

$$u(\mathbf{x}, 0) = \psi_0(\mathbf{x}), \quad \partial_t u(\mathbf{x}, 0) = \Omega \nabla \psi_0(\mathbf{x}) \begin{pmatrix} y \\ -x \end{pmatrix} + \frac{1}{\varepsilon^2} \psi_1(\mathbf{x}), \quad \mathbf{x} \in [-a, a] \times [-b, b], \quad (3.11b)$$

$$u(a, y, t) = u(-a, y, t), \quad \partial_x u(a, y, t) = \partial_x u(-a, y, t), \quad y \in [-b, b], \quad t \geq 0, \quad (3.11c)$$

$$u(x, b, t) = u(x, -b, t), \quad \partial_y u(x, b, t) = \partial_y u(x, -b, t), \quad x \in [-a, a], \quad t \geq 0. \quad (3.11d)$$

We consider (3.11) for a wide range of the ‘‘non-relativistic’’ parameter $0 < \varepsilon \leq 1$. Since (3.11) reads as a standard cubic Klein-Gordon equation, many numerical methods in the literature could apply. Here to solve (3.11) with robustness on $0 < \varepsilon \leq 1$, we shall consider two multiscale numerical integrators. One is the uniformly accurate (UA) exponential integrator (EI) and the other is the multi-revolution composition (MRC) method. MRC applies when $V(\mathbf{x})$ is isotropic and the scheme is geometric which provides good behaviour in long-time computing [22]. EI applies in general (anisotropic $V(\mathbf{x})$) and the scheme is optimal in computational cost [15]. Both methods give approximations with uniform accuracy for all $0 < \varepsilon \leq 1$. That is to say the schemes can capture accurately the dynamics in the rotating cosmic superfluid and its transition to the rotating BEC in the non-relativistic limit under the same computational cost.

Multi-revolution composition method. The multi-revolution composition (MRC) method applies when the trapping potential in (3.11) is *isotropic*, so $V(A(t)\mathbf{x}) = V(\mathbf{x})$. The MRC method is originally proposed in [22] as a general geometric framework for autonomous highly oscillatory problems. It has been applied to solve oscillatory nonlinear Schrödinger equation [23] and recently to Vlasov equation [21]. Particularly in [21], MRC has been revealed to give uniform accuracy in terms of the oscillation frequency. We shall for the first time apply this method to solve the RKG by firstly perform a suitable reformulation of (3.11).

Introduce unknowns w_{\pm} :

$$w_+(\mathbf{x}, t) := u(\mathbf{x}, t) - i\varepsilon^2 A_\varepsilon \partial_t u(\mathbf{x}, t), \quad w_-(\mathbf{x}, t) := \bar{u}(\mathbf{x}, t) - i\varepsilon^2 A_\varepsilon \partial_t \bar{u}(\mathbf{x}, t), \quad (3.12)$$

and operators

$$A_\varepsilon := \frac{1}{\sqrt{1 - \varepsilon^2 \Delta}}, \quad D_\varepsilon := \frac{1}{\varepsilon^2} \left[\sqrt{1 - \varepsilon^2 \Delta} - 1 \right].$$

Then the RKG (3.11) can be written as

$$i\partial_t w_{\pm}(\mathbf{x}, t) = -\frac{1}{\varepsilon^2} w_{\pm}(\mathbf{x}, t) + F_{\pm}(w_+(\mathbf{x}, t), w_-(\mathbf{x}, t)), \quad (3.13)$$

with

$$F_{\pm}(w_+, w_-) = -D_\varepsilon w_{\pm} - A_\varepsilon \left[\frac{\lambda}{8} |w_{\pm} + \bar{w}_{\mp}|^2 + \frac{V}{2} \right] (w_{\pm} + \bar{w}_{\mp}).$$

It is clear to see that the pseudo-differential operators satisfy

$$0 < A_\varepsilon \leq 1, \quad 0 \leq D_\varepsilon \leq -\frac{\Delta}{2}.$$

Suppose that we are solving RKG (3.11) till time $T_f > 0$. Then by a rescaling of the time $t \rightarrow \varepsilon^2 t$, we rewrite (3.13) as

$$i\partial_t w_\pm(\mathbf{x}, t) = -w_\pm(\mathbf{x}, t) + \varepsilon^2 F_\pm(w_+(\mathbf{x}, t), w_-(\mathbf{x}, t)), \quad 0 < t \leq \frac{T_f}{\varepsilon^2}, \quad (3.14a)$$

$$w_+(\mathbf{x}, 0) = u(\mathbf{x}, 0) - i\varepsilon^2 A_\varepsilon \partial_t u(\mathbf{x}, 0), \quad w_-(\mathbf{x}, 0) = \bar{u}(\mathbf{x}, 0) - i\varepsilon^2 A_\varepsilon \partial_t \bar{u}(\mathbf{x}, 0), \quad (3.14b)$$

on the periodic box $(-a, a) \times (-b, b)$ for \mathbf{x} .

Clearly, we see the linear part of (3.14) generates a 2π -periodic flow and the nonlinear part is bounded as $\varepsilon \rightarrow 0$. Now we write the final time as

$$\frac{T_f}{\varepsilon^2} = 2\pi M_f + T_r, \quad M_f = \frac{T_f}{2\pi\varepsilon^2} \in \mathbb{N}, \quad 0 \leq T_r < 2\pi.$$

The 2nd order MRC method begins by choosing an integer $0 < M_0 \leq M_f$ with

$$\alpha = \frac{1}{2} \left(1 + \frac{1}{M_0} \right), \quad \beta = \frac{1}{2} \left(1 - \frac{1}{M_0} \right), \quad N = \frac{M_f}{M_0}, \quad H = \varepsilon^2 M_0,$$

denoting $w_\pm^n \approx w_\pm(2\pi n M_0)$, and then the MRC scheme proceeds as

$$\begin{pmatrix} w_+^{n+1} \\ w_-^{n+1} \end{pmatrix} = \mathcal{E}_\beta(-2\pi) \mathcal{E}_\alpha(2\pi) \begin{pmatrix} w_+^n \\ w_-^n \end{pmatrix}, \quad 0 \leq n \leq N-1, \quad (3.15)$$

where $\mathcal{E}_\alpha(2\pi)$ denotes the flow:

$$i\partial_t w_\pm = -w_\pm + \alpha H F_\pm(w_+, w_-), \quad 0 < t \leq 2\pi, \quad (3.16)$$

and $\mathcal{E}_\beta(-2\pi)$ denotes the flow:

$$i\partial_t w_\pm = -w_\pm - \beta H F_\pm(w_+, w_-), \quad -2\pi \leq t < 0. \quad (3.17)$$

After evaluating (3.15) till $n = N$, the MRC method is completed by solving the remaining flow $\mathcal{E}_r(T_r)$:

$$i\partial_t w_\pm = -w_\pm + \varepsilon^2 F_\pm(w_+, w_-), \quad 0 < t \leq T_r. \quad (3.18)$$

To further integrate the sub-flow (3.16), (3.17) or (3.18), we use a Strang splitting scheme. For example for $\mathcal{E}_\alpha(2\pi)$ (similarly for others):

$$i\partial_t w_\pm = (-1 - \alpha H D_\varepsilon) w_\pm - \alpha H A_\varepsilon \left[\frac{\lambda}{8} |w_\pm + \bar{w}_\mp|^2 + \frac{V}{2} \right] (w_\pm + \bar{w}_\mp),$$

we split the flow as

$$\mathcal{E}_\alpha^k(t) : i\partial_t w_\pm = (-1 - \alpha H D_\varepsilon) w_\pm \quad \text{and} \quad \mathcal{E}_\alpha^p(t) : i\partial_t w_\pm = -\alpha H A_\varepsilon \left[\frac{\lambda}{8} |w_\pm + \bar{w}_\mp|^2 + \frac{V}{2} \right] (w_\pm + \bar{w}_\mp).$$

Noting that $w_\pm + \bar{w}_\mp$ is time-independent in $\mathcal{E}_\alpha^k(t)$, both $\mathcal{E}_\alpha^k(t)$ and $\mathcal{E}_\alpha^p(t)$ can be evaluated exactly. The exact solution of $\mathcal{E}_\alpha^k(t)$ is

$$w_\pm(\mathbf{x}, t) = e^{it(1+\alpha H D_\varepsilon)} w_\pm(\mathbf{x}, 0), \quad t > 0,$$

and the exact solution of $\mathcal{E}_\alpha^p(t)$ is

$$w_\pm(\mathbf{x}, t) = w_\pm(\mathbf{x}, 0) + it\alpha H A_\varepsilon \left[\frac{\lambda}{8} |w_\pm(\mathbf{x}, 0) + \bar{w}_\mp(\mathbf{x}, 0)|^2 + \frac{V}{2} \right] (w_\pm(\mathbf{x}, 0) + \bar{w}_\mp(\mathbf{x}, 0)), \quad t > 0.$$

We take the same integer N to discretize the time interval $[0, 2\pi]$ of the subflow $\mathcal{E}_\alpha(2\pi)$ and denote the (micro) time step size as $h = 2\pi/N$. Then $\mathcal{E}_\alpha(2\pi)$ is approximated by the Strang splitting:

$$\mathcal{E}_\alpha(2\pi) \approx (\mathcal{E}_\alpha^p(h/2) \mathcal{E}_\alpha^k(h) \mathcal{E}_\alpha^p(h/2))^N.$$

It is worth noting that when M_0 decreases to the critical value $M_0 = 1$, we have $\alpha = 1, \beta = 0$ in the MRC scheme and hence $\mathcal{E}_\beta(-2\pi)$ becomes identity. It means that MRC automatically reduces

to direct integration on the flow (3.14) with the Strang splitting scheme under the time step $\Delta t = h$. Therefore, adopting the strategy proposed in [21], for some given integer $N > 0$ (the number of macro grids, which is the preferred user controlled parameter in practice) such that $M_0 = T_f/\varepsilon^2/(2\pi N) < 1$, we shall consider the MRC scheme as the direct Strang splitting scheme on (3.14) with time step $\Delta t = h = 2\pi/N$ accomplished by the remaining flow (3.18). With w_{\pm}^n from the MRC scheme (3.15), one gets the numerical solution of RKG by

$$u(\mathbf{x}, t_n) \approx u^n = \frac{1}{2} (w_+^n + \bar{w}_-^n), \quad \partial_t u(\mathbf{x}, t_n) \approx u_t^n = \frac{i}{2\varepsilon^2 A_\varepsilon} (w_+^n - \bar{w}_-^n). \quad (3.19)$$

In practice, the involved spatial differentiations A_ε and D_ε in the MRC scheme could be computed by the Fourier pseudo-spectral discretization in the bounded space interval I under spatial step size $\Delta x, \Delta y > 0$.

The MRC framework is a geometric method which guarantees good long-time behavior of the method. Moreover, the proposed MRC scheme is charge-preserving.

Lemma 3.2. *The proposed MRC scheme (3.15)-(3.19) preserves the charge (1.6) of the RKG at the discrete time level in the Lagrangian coordinates.*

Proof. Under the coordinates change (3.8) and reformulation (3.12), the charge (1.6) in terms of the new variables in the Lagrange coordinates read as

$$Q(t) = \frac{1}{4} \int_{\mathbb{R}^2} \operatorname{Re} [(w_+(\mathbf{x}, t) + \bar{w}_-(\mathbf{x}, t)) A_\varepsilon^{-1} (\bar{w}_+(\mathbf{x}, t) - w_-(\mathbf{x}, t))] d\mathbf{x}.$$

Note that the MRC scheme is a composition of sub-flows such as $\mathcal{E}_\alpha^k(t)$ and $\mathcal{E}_\beta^k(t)$, where the sub-flows are exactly integrated. Hence, the rest part of the proof is by directly checking that $\mathcal{E}_\alpha^k(t)$ and $\mathcal{E}_\beta^k(t)$ (same to the others) preserve the charge. \square

Noting that the linear part of the flow in (3.14) is isometric, so provided that the solution of (3.14) is sufficiently smooth and using similar proof strategy in [23], the temporal error of the MRC method at a fixed time can be shown to have a super convergence in terms of ε , and the optimal total error bound thus reads:

$$O(H^2) + O(\varepsilon^2 h^2) + O(\Delta x^{m_0}) + O(\Delta y^{m_0}),$$

where $m_0 > 0$ depends on the smoothness of the solution in space. MRC is temporally second order accurate with respect to the number of macro time grid points N (noting $H, h = O(N^{-1})$) and spectrally accurate in space discretization.

UA exponential integrator. As another uniformly accurate (UA) method, the exponential integrator (EI) proposed in [15] for solving the nonlinear Klein-Gordon equation in the non-relativistic limit regime can be applied to handle *general potential* function V case, e.g. non-symmetric or time-dependent. The scheme is optimal in computational costs compared to the other UA methods [3, 20, 21]. The scheme gets very complicated at high order versions particularly when the solution of the Klein-Gordon equation is complex-valued. Here to study the vortices dynamics in (3.11), we need to consider complex-valued initial values ψ_0, ψ_1 for (3.11) in order to have non-zero charge. Therefore, to make an application of the EI scheme for (3.11), we write down the first order scheme under the complex-valued case with a brief derivation.

Based on (3.13), we further introduce the filtered variables

$$v_+(\mathbf{x}, t) := e^{-it/\varepsilon^2} (u(\mathbf{x}, t) - i\varepsilon^2 A_\varepsilon \partial_t u(\mathbf{x}, t)), \quad v_-(\mathbf{x}, t) := e^{-it/\varepsilon^2} (\bar{u}(\mathbf{x}, t) - i\varepsilon^2 A_\varepsilon \partial_t \bar{u}(\mathbf{x}, t)),$$

then the RKG (3.11) can be written as

$$i\partial_t v_{\pm} = -D_\varepsilon v_{\pm} - A_\varepsilon e^{-it/\varepsilon^2} \left[\frac{\lambda}{8} \left| e^{it/\varepsilon^2} v_{\pm} + e^{-it/\varepsilon^2} \bar{v}_{\mp} \right|^2 + \frac{V(A(t)\mathbf{x})}{2} \right] \left(e^{it/\varepsilon^2} v_{\pm} + e^{-it/\varepsilon^2} \bar{v}_{\mp} \right).$$

By Duhamel's principle for some $n \geq 0$, one gets (drop \mathbf{x} for simplicity)

$$\begin{aligned} v_{\pm}(t_{n+1}) &= \frac{iA_{\varepsilon}}{8} \int_0^{\Delta t} e^{i(\Delta t - \theta)D_{\varepsilon} - i(t_n + \theta)/\varepsilon^2} \lambda \left(e^{i(t_n + \theta)/\varepsilon^2} v_{\pm}(t_n + \theta) + e^{-i(t_n + \theta)/\varepsilon^2} \overline{v_{\mp}}(t_n + \theta) \right) \\ &\quad \times \left[4V(A(t_n + \theta)\mathbf{x}) + \left| e^{i(t_n + \theta)/\varepsilon^2} v_{\pm}(t_n + \theta) + e^{-i(t_n + \theta)/\varepsilon^2} \overline{v_{\mp}}(t_n + \theta) \right|^2 \right] d\theta + e^{i\Delta t D_{\varepsilon}} v_{\pm}(t_n). \end{aligned} \quad (3.20)$$

The first order scheme completes by approximating $A(t_n + \theta) \approx A(t_n)$, $v_{\pm}(t_n + \theta) \approx v_{\pm}(t_n)$ and then carrying out the integration exactly.

In details, denoting $v_{\pm}^n(\mathbf{x}) \approx v_{\pm}(\mathbf{x}, t_n)$, the EI scheme reads for $n \geq 0$,

$$\begin{aligned} v_{\pm}^{n+1} &= e^{i\Delta t D_{\varepsilon}} v_{\pm}^n + e^{2it_n/\varepsilon^2} c_1 \lambda (v_{\pm}^n)^2 v_{\mp}^n + c_2 [\lambda (|v_{\pm}^n|^2 + 2|v_{\mp}^n|^2) + 4V(A(t_n)\mathbf{x})] v_{\pm}^n \\ &\quad + e^{-2it_n/\varepsilon^2} c_3 [\lambda (|v_{\mp}^n|^2 + 2|v_{\pm}^n|^2) + 4V(A(t_n)\mathbf{x})] \overline{v_{\mp}^n} + e^{-4it_n/\varepsilon^2} c_4 \lambda \overline{v_{\pm}^n (v_{\mp}^n)^2}, \end{aligned} \quad (3.21)$$

with

$$\begin{aligned} c_1 &= \varepsilon^2 A_{\varepsilon} \frac{e^{2i\Delta t/\varepsilon^2} - e^{iD_{\varepsilon}\Delta t}}{16 - 8\varepsilon^2 D_{\varepsilon}}, & c_2 &= A_{\varepsilon} \frac{e^{iD_{\varepsilon}\Delta t} - 1}{8D_{\varepsilon}}, \\ c_3 &= \varepsilon^2 A_{\varepsilon} \frac{e^{iD_{\varepsilon}\Delta t} - e^{-2i\Delta t/\varepsilon^2}}{16 + 8D_{\varepsilon}\varepsilon^2}, & c_4 &= \varepsilon^2 A_{\varepsilon} \frac{e^{iD_{\varepsilon}\Delta t} - e^{-4i\Delta t/\varepsilon^2}}{32 + 8D_{\varepsilon}\varepsilon^2}. \end{aligned}$$

The approximation to the solution of RKG (3.11) would be

$$u(\mathbf{x}, t^n) \approx \frac{1}{2} \left[e^{it_n/\varepsilon^2} v_+^n(\mathbf{x}) + e^{-it_n/\varepsilon^2} \overline{v_-^n(\mathbf{x})} \right].$$

The above involved spatial differentiations could also be done by the Fourier discretization in space. Up to a fixed time, the error of the EI scheme (3.21) is

$$O(\Delta t) + O(\Delta x^{m_0}) + O(\Delta y^{m_0}).$$

To get higher order EI schemes with uniform accuracy for $\varepsilon \in (0, 1]$, we remark that standard high order quadratures [32, 35] can not be applied to (3.20), since the integral has a highly oscillatory kernel function with ε -dependent frequency and the unknowns have unbounded second order time derivatives as $\varepsilon \rightarrow 0$, i.e. $\partial_{tt} v_{\pm} = O(\varepsilon^{-2})$. This will be further addressed by numerical results later. One option for high order uniformly accurate EI schemes as proposed in [15] is to use a Picard iteration, which even at second order becomes very involved and was only done for real-valued nonlinear Klein-Gordon equation in [15].

Remark 3.3. In 3D, the rotating Lagrangian coordinates can be introduced in the same way as presented above by defining the rotating matrix

$$A(t) = \begin{pmatrix} \cos(\Omega t) & \sin(\Omega t) & 0 \\ -\sin(\Omega t) & \cos(\Omega t) & 0 \\ 0 & 0 & 1 \end{pmatrix}.$$

The extensions of MRC method and EI in 3D are straightforward.

4. NUMERICAL RESULTS

In this section, we present the convergence results of the proposed numerical methods and the simulation results of the vortices dynamics in the RKG (1.3) for $0 < \varepsilon \leq 1$.

4.1. Accuracy test. Here we test the convergence of the proposed methods. We take a 2D example in (1.3), i.e. $d = 2$, $\mathbf{x} = (x, y)$,

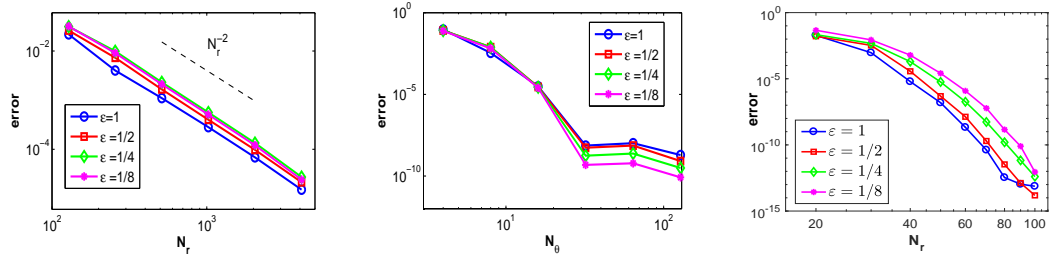
$$\Omega = 1, \quad \lambda = 0.5, \quad V(\mathbf{x}) = \frac{|\mathbf{x}|^2}{2} e^{-|\mathbf{x}|^2}, \quad \psi_0(\mathbf{x}) = e^{-2x^2 - 1.5y^2} \frac{x + iy}{|\mathbf{x}|^2 + 1}, \quad \psi_1(\mathbf{x}) = i\psi_0(\mathbf{x}), \quad (4.1)$$

and solve the problem till $T = \pi/4$.

Accuracy confirmation of SIFS. In polar coordinates, the computational domain is chosen as the disk of radius $R_0 = 10$ centered at the origin. We shall test the temporal and spatial accuracy

TABLE 2. Temporal error of SIFS in $\Delta t = T/N$ under different ε .

	$N = 128$	$N * 2$	$N * 2^2$	$N * 2^3$	$N * 2^4$	$N * 2^5$
$\varepsilon = 1$	6.16E-3	1.56E-3	3.93E-4	9.84E-5	2.44E-5	5.81E-6
rate	-	1.98	1.99	2.00	2.01	2.07
$\varepsilon = 1/2$	8.06E-2	2.05E-2	5.15E-3	1.29E-3	3.19E-4	7.61E-5
rate	-	1.98	1.99	2.00	2.01	2.07
$\varepsilon = 1/4$	8.51E-1	2.47E-1	6.27E-2	1.57E-2	3.88E-3	9.26E-4
rate	-	1.78	1.98	2.00	2.01	2.07
$\varepsilon = 1/8$	5.77	8.78E-1	1.66	4.66E-1	1.16E-1	2.78E-2
rate	-	2.72	-0.92	1.83	2.00	2.07

FIGURE 2. Error of SIFS with respect to the number of spatial grids N_r (left) and N_θ (middle) under different ε , and the corresponding error of Chebyshev+Fourier method for radius direction with respect to N_r (right).

(in both r and θ -directions) for different ε . The benchmark solution is obtained with fine mesh $\Delta t = T/2^{14}$, $N_r = 2048$ in the r -direction and $N_\theta = 128$ in the θ -direction. For the temporal error test, we fix grid points $N_r = 2048$ and $N_\theta = 128$ such that errors coming from the r and θ are negligible, and we compute the errors with different number of time grids $N = T/\Delta t$. The relative maximum error in Ψ and the corresponding convergence rates are presented in Tab. 2. We see that under a fixed N , the error of SIFS increases dramatically as ε decreases and the method loses its efficiency in the limit regime.

To confirm the spatial accuracy in the r -direction, we choose $N_\theta = 128$, $\Delta t = T/2^{14}$ such that errors from θ and Δt are negligible, and compute the relative maximum for different N_r . Fig. 2 (the second figure) displays the spatial error in r -direction, together with convergence rates, for different ε . The spectral accuracy in the θ -direction is confirmed by Fig. 2, where we use the same fine mesh and time step as $N_r = 2048$, $\Delta t = T/2^{14}$ for different ε . In addition, we also show in Fig. 2 the error of using the Chebyshev method from Remark 3.1 as the alternative in SIFS for discretization in the r -direction to illustrate the uniform spectral accuracy, where we calculated the successive maximum error, with $T = 1/4$, $\Delta t = 1/200$, $N_\theta = 64$.

Uniform accuracy confirmation of MRC and EI. For the MRC and EI methods in Cartesian coordinates, we take the truncated square domain as $I = (-8, 8)^2$. The reference solution is obtained by MRC with very small step size. To study the temporal error of the two methods, we fix the number of grids $M = 256$ to discretize the space x or y -direction (i.e. $\Delta x = \Delta y = 1/16$) such that the discretization error is negligible. The error of EI in the solution Ψ at $t = T$ under maximum norm with respect to the number of grids $N = T/\Delta t$ in time is shown in Fig. 3 under different ε , and the corresponding error of MRC with respect to N is shown Fig. 4. For comparison purpose, we implement a classical fourth order symmetric Gautschi-type exponential integrator [35, 65] which is non-uniformly accurate, and its error in Ψ under maximum norm is listed in Tab. 3. To study the spatial discretization error of MRC and EI, we fix the number of the temporal grids $N = 512$ and plot the error under maximum norm with respect to M . The errors are shown in Fig. 5.

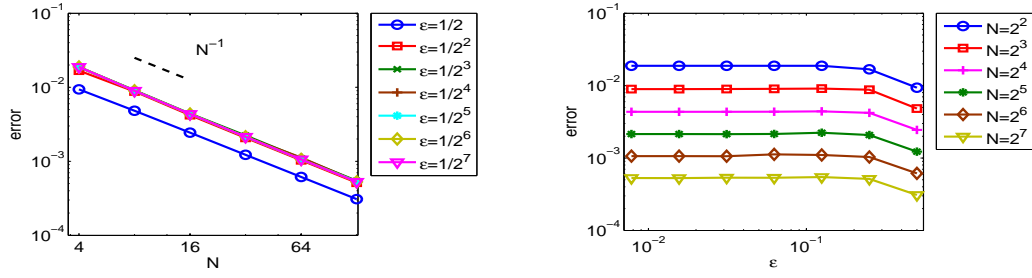


FIGURE 3. Error of EI with respect to the number of temporal grids N under different ε .

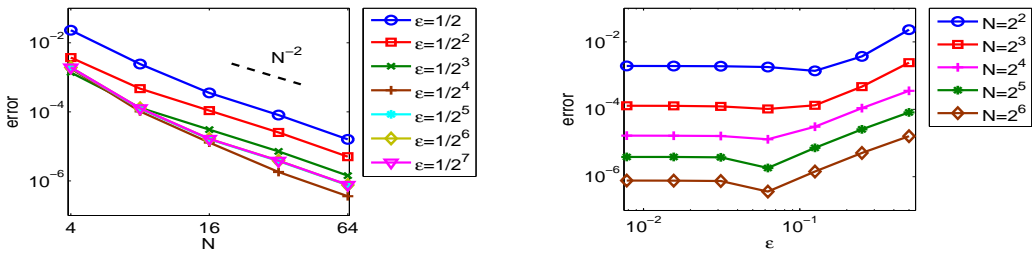


FIGURE 4. Error of MRC with respect to the number of (macro) temporal grids N under different ε .

TABLE 3. Temporal error of 4th order classical exponential integrator in $\Delta t = T/N$ under different ε ('Inf' denotes numerical blow-up due to $\Delta t > \varepsilon^2$).

	$N = 4$	$N * 2$	$N * 2^2$	$N * 2^3$	$N * 2^4$	$N * 2^5$
$\varepsilon = 1/2$	3.25E-4	1.35E-5	3.63E-7	2.15E-8	1.32E-9	7.76E-11
rate	-	4.59	5.21	4.08	4.02	4.09
$\varepsilon = 1/4$	1.77E-2	1.80E-3	1.63E-5	7.33E-7	4.44E-8	2.59E-9
rate	-	3.29	6.79	4.47	4.04	4.09
$\varepsilon = 1/8$	4.93E-1	4.70E-1	3.98E-2	1.31E-4	6.08E-6	3.34E-7
rate	-	0.07	3.56	8.24	4.43	4.18
$\varepsilon = 1/16$	3.23E+5	Inf	Inf	Inf	1.01E-1	1.14E-4
rate	-	-	-	-	-	9.79

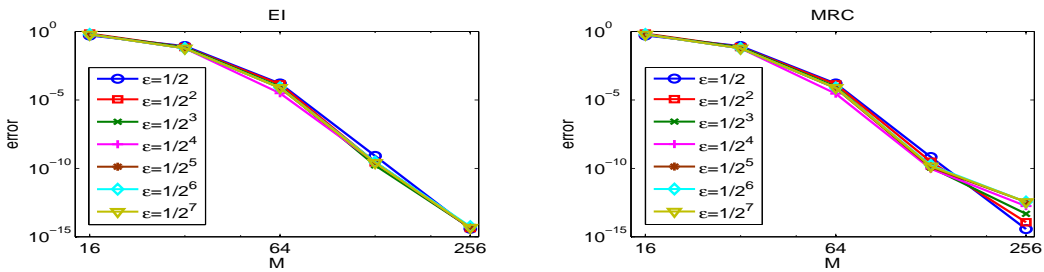


FIGURE 5. Error of EI and MRC with respect to the number of spatial grids (in x or y) M under different ε .

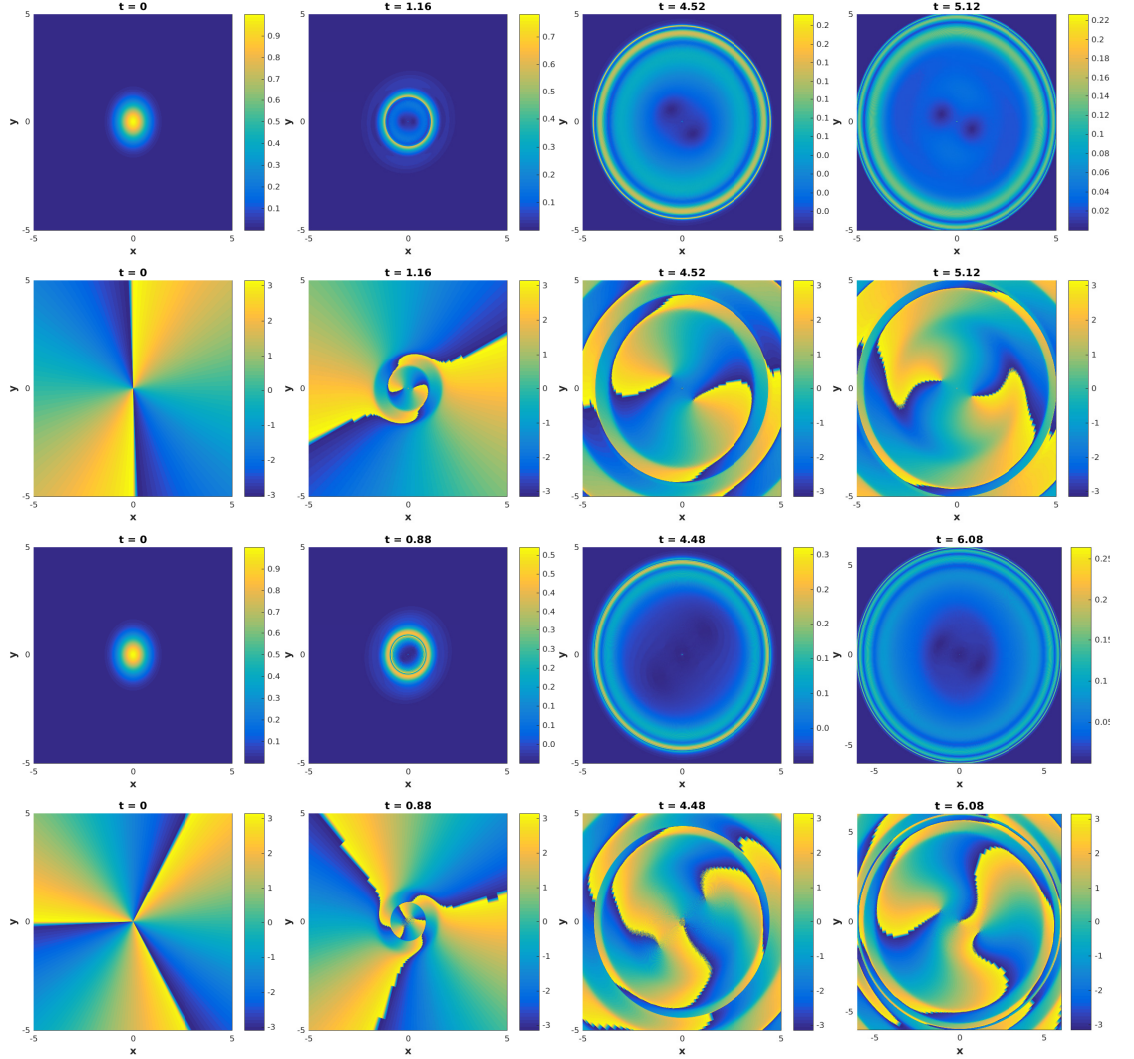


FIGURE 6. Contour plot of $|\Psi(\mathbf{x}, t)|$ and $\text{Arg}(\Psi)(\mathbf{x}, t)$ at different times with $N_0 = 2$ (the first two rows) and $N_0 = 3$ (the last two rows).

From the numerical results, we see that the error of both EI and MRC converge in time and also in space uniformly for all $0 < \varepsilon \leq 1$. In particular, EI is uniformly first order accurate in time and MRC is uniformly second order with respect to the macro grids N . In contrast, the classical m -th order integrators has temporal error $O(\tau^m/\varepsilon^{2m})$ due to the essential $O(\varepsilon^2)$ -wavelength in time. Although $m \in \mathbb{N}$ could be arbitrarily large, the mesh strategy $\tau \lesssim \varepsilon^2$ must always be satisfied for convergence, which makes the efficiency of classical integrators not comparable to the proposed uniformly accurate methods when ε becomes small. When $\tau > \varepsilon^2$, numerical instability could occur even for linearly stable schemes [5, 12]. This can clearly be seen by comparing Tab. 3 with Figs. 3&4. For a more systematical comparisons between classical integrators and uniformly accurate methods, we refer to [12]. In space, MRC and EI are uniformly spectrally accurate. The uniformly accurate property of MRC and EI allow to use large mesh size which certainly increases the efficiency of simulations compared to the algorithm in polar coordinates and other classical integrators.

4.2. Simulations. Now, we apply the proposed numerical methods for simulating the vortices dynamics in the RKG (1.3) ranging from the relativistic regime to the non-relativistic regime.

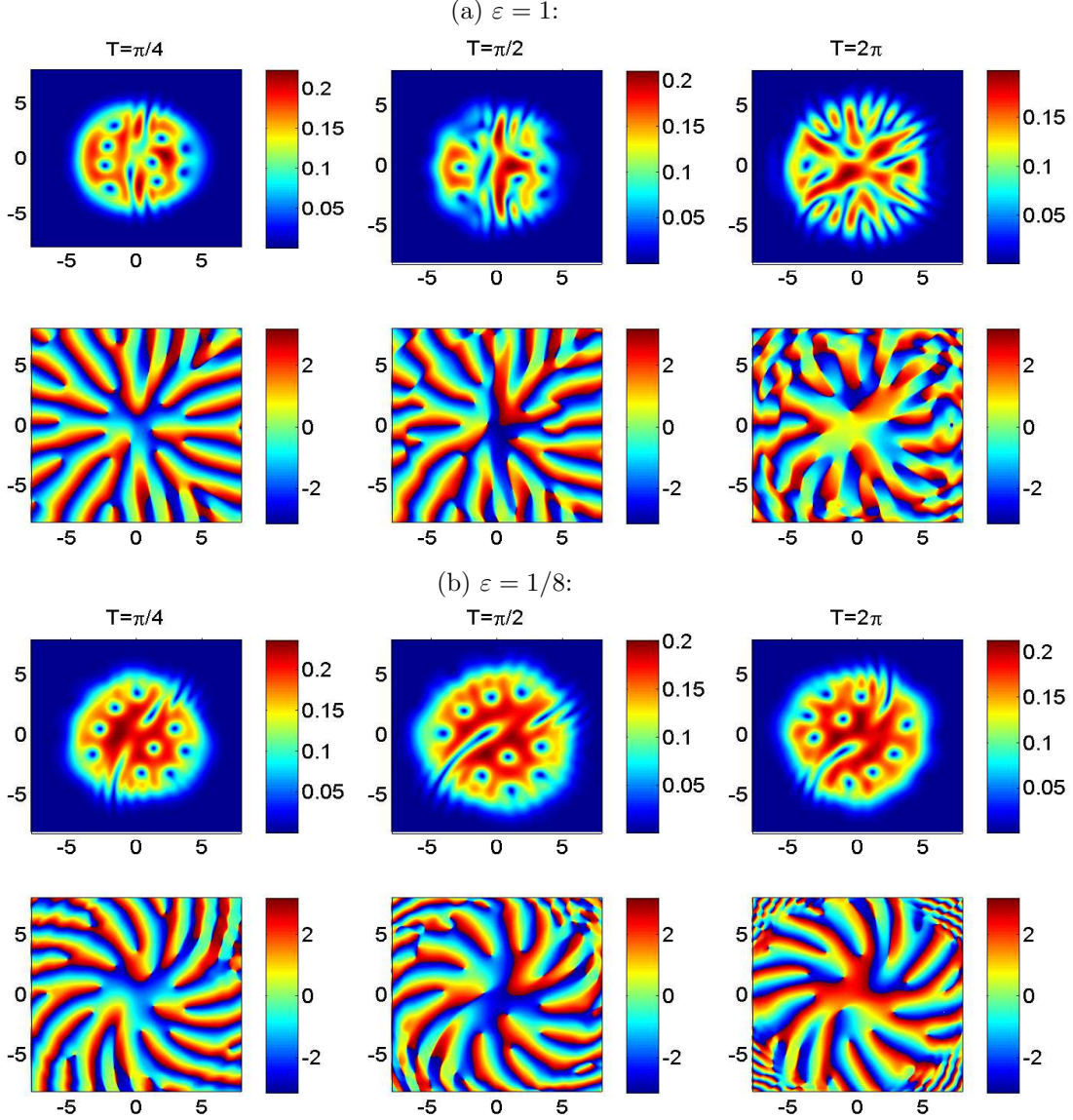


FIGURE 7. Contour plot of $|\Psi|$ and $\text{Arg}(\Psi)$ in example 4.2 under: (a) $\varepsilon = 1$; (b) $\varepsilon = 1/8$.

Example 4.1. (*Vortices creation*) For the first example, we investigate the generation of vortices in the RKG in the classical scaling, i.e. $\varepsilon = 1$. As a valid rotating model, vortices can be generated in the RKG (1.3) by taking a non-symmetric initial data with non-zero charge. This phenomenon obeys the relativistic Feynman relation and has been observed for the RKG (1.3) in the relativistic regime on a disk domain in [62, 31]. Here to simulate this phenomenon and verify the observation from [62, 31], we consider (1.3) with $\varepsilon = 1$ on a disk. We take the initial values as

$$\psi_0(\mathbf{x}) = \rho_0(\mathbf{x})e^{iN_0\theta}, \quad \psi_1 = i\omega\psi_0(\mathbf{x}),$$

with $\rho_0(\mathbf{x})$ as an anisotropic Gaussian, $N_0 \in \mathbb{N}^+$ and $\omega \in \mathbb{R}^+$, and we apply the SIFS method to solve the RKG (1.3).

The numerical simulation is carried out on a disk of radius $R_0 = 10$ with $N_\theta = 128$, $N_r = 2048$ and $\Delta t = 10^{-4}$ for $\Omega = 1$, $\lambda = 2$ under potential $V = r^2$. The initial anisotropic distribution is chosen as $\rho_0 = e^{-2x^2 - 1.5y^2}$ with $\omega = 1$ and $N_0 = 2$ or 3. In Fig. 6, we can see that clearly there are

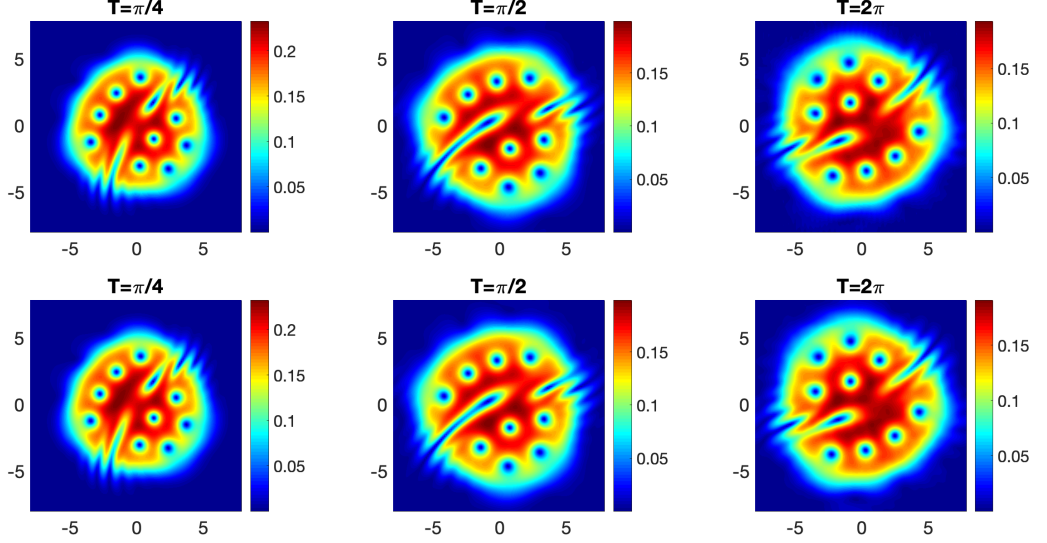


FIGURE 8. $|\Psi|$ of RKG under $\varepsilon = 1/32$ and $|e^{it/\varepsilon^2} z_+ + e^{-it/\varepsilon^2} \bar{z}_-|$ from RNLS in example 4.2.

no vortices initially, but as time evolves, some vortices will be created during the dynamics. The maximum number of vortices that could be generated equals to N_0 .

Example 4.2. (*Relativistic effect on the bound state*) Next, we investigate how the vortices pattern from the RNLS model gets affected by the relativistic effect. To this purpose, we take the bound state z_{\pm} of the RNLS (2.7) obtained in Fig. 1 and input it as the initial value of the RKG (1.4) as

$$\psi_0(\mathbf{x}) = z_+(\mathbf{x}) + \bar{z}_-(\mathbf{x}), \quad \psi_1(\mathbf{x}) = i(z_+(\mathbf{x}) - \bar{z}_-(\mathbf{x})),$$

which is asymptotically consistent with expansion (2.1) as $\varepsilon \rightarrow 0$. The other computational setups for RKG (1.3) are the same as for the bound state, i.e. $\lambda = 50$, $V = \frac{1}{2}(x^2 + y^2)$ and $\Omega = 0.9$. We solve the RKG under different ε in the rotating Lagrangian coordinates by MRC. The solutions $\Psi(\mathbf{x}, t)$ of RKG under $\varepsilon = 1$ and $\varepsilon = 1/8$ at different time are shown in Fig. 7. Furthermore, Fig. 8 shows the solution Ψ of RKG under $\varepsilon = 1/32$ and the direct result from the RNLS model:

$$e^{it/\varepsilon^2} z_+(\mathbf{x}) + e^{-it/\varepsilon^2} \bar{z}_-(\mathbf{x}).$$

Note that all the solutions here are plotted in the rotating Lagrangian coordinates.

From the results we see that when $\varepsilon = 1$, the relativistic effect does a strong modification to the vortices pattern as time evolves. As ε becomes small, the vortices pattern maintains well in the dynamics and rotates with time. When $\varepsilon \rightarrow 0$, the dynamical configuration from RKG is closed to the result from the RNLS model, which again justifies the convergence between the two models in the non-relativistic limit.

Example 4.3. (*Interaction of vortex pairs*) In the last but not least example, we investigate the interaction of vortices in RKG in the non-relativistic limit regime. To do so, we input two pairs of initially well-separated vortices in the RKG (1.3) in two dimensions and consider their dynamics under different ε . We take the parameters in the equation (1.3) as

$$\Omega = 0.5, \quad \lambda = 10,$$

and the initial data as two vortex pairs:

$$\psi_0(\mathbf{x}) = \psi_1(\mathbf{x}) = (x - c_0 + iy)(x + c_0 + iy)(x + i(y - c_0))(x + i(y + c_0))e^{-(x^2 + y^2)/2},$$

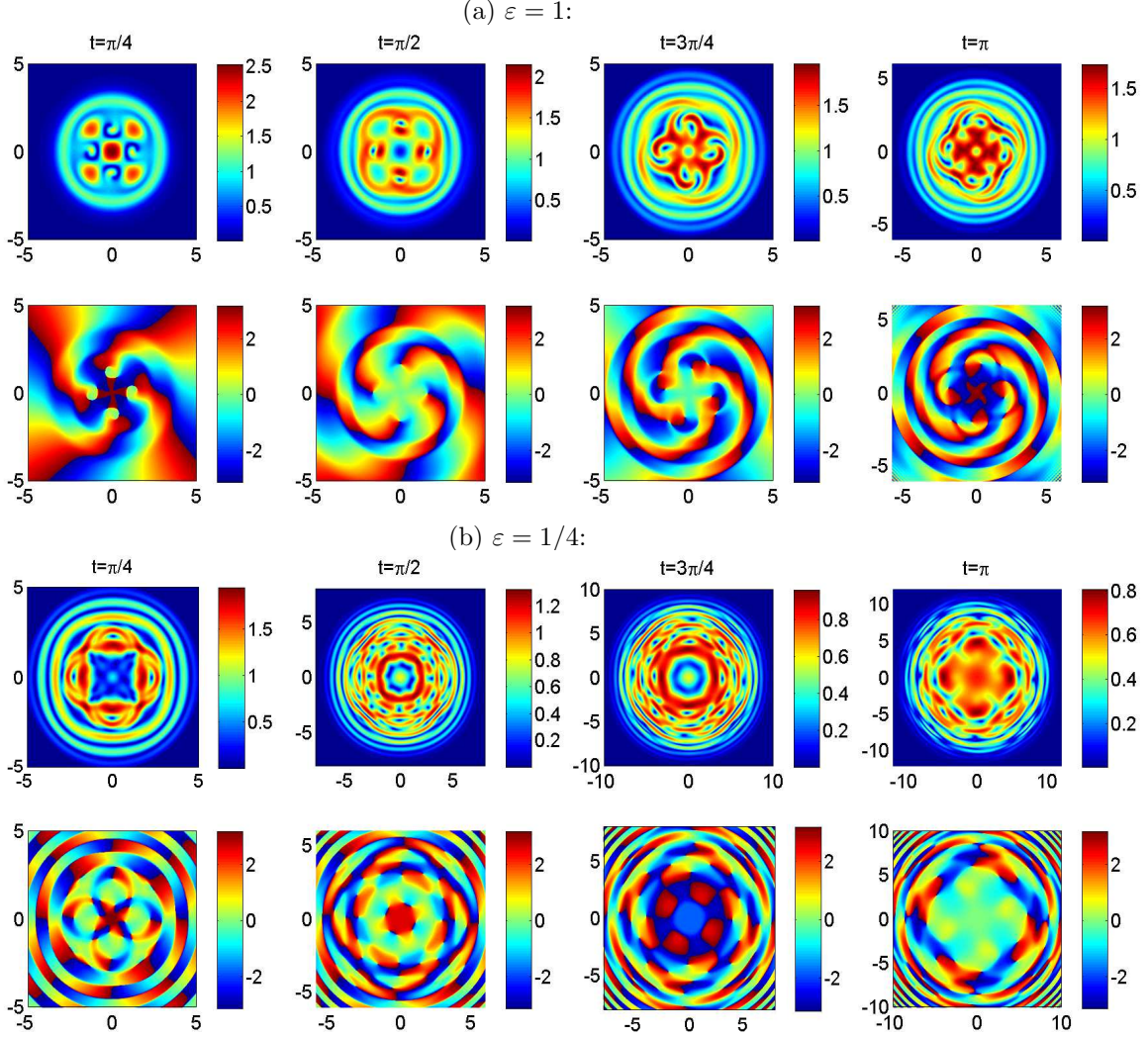


FIGURE 9. Contour plot of $|\Psi|$ and $\text{Arg}(\Psi)$ in example 4.3 with symmetric potential under: (a) $\varepsilon = 1$; (b) $\varepsilon = 1/4$.

with $c_0 = 1.32$. Considering the symmetric potential case:

$$V(\mathbf{x}) = \frac{1}{2}(x^2 + y^2),$$

we solve the problem under different ε by MRC in the Lagrangian coordinates on domain $(-32, 32)^2$ till $t = \pi$. In Fig. 9, the solution $|\Psi(\mathbf{x}, t)|$ and $\text{Arg}(\Psi(\mathbf{x}, t))$ are plotted at different time t under $\varepsilon = 1, 1/4$. Fig. 10 shows the result under $\varepsilon = 1/16$. The time evolutions of the numerical energy $E^n \approx E(t_n)$ and the numerical charge $Q^n \approx Q(t_n)$ given by the scheme during the simulation are shown in Fig. 11. For a non-symmetric potential case:

$$V(\mathbf{x}) = 0.5x^2 + 1.5y^2,$$

we solve the problem by EI and the results under $\varepsilon = 1/4$ are shown in Fig. 12.

From the numerical results we can see that when ε gets smaller in the non-relativistic limit, the interactions between the vortices get stronger, and many detailed structures are generated in the configurations as time evolves. During our computations by MRC in the symmetric potential case,

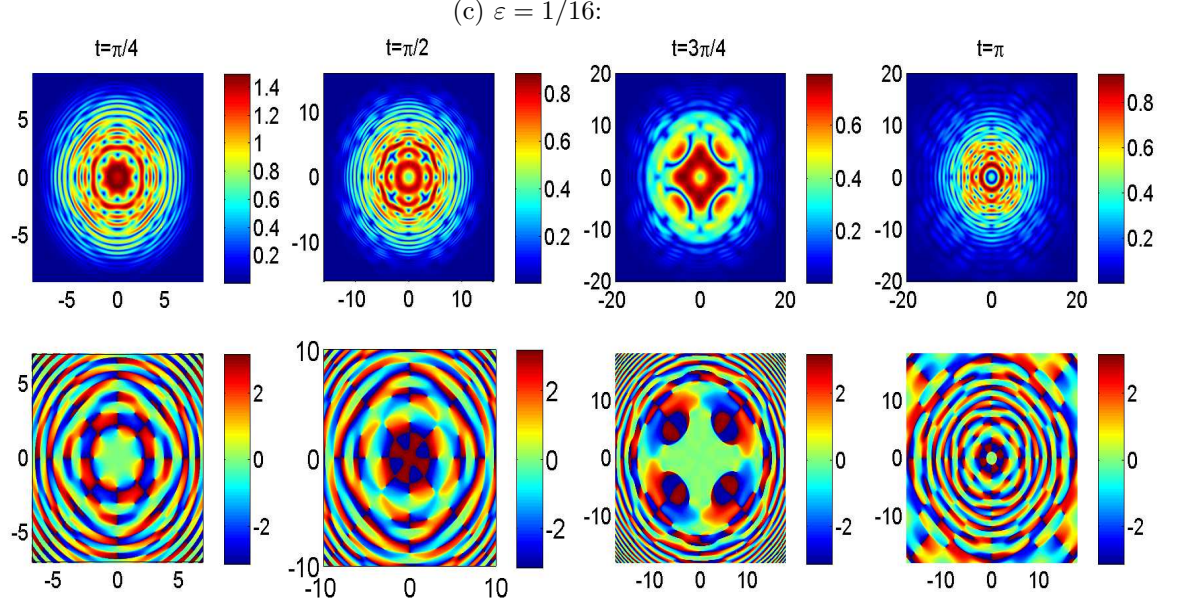


FIGURE 10. Contour plot of $|\Psi|$ and $\text{Arg}(\Psi)$ in example 4.3 with symmetric potential at different t under: (c) $\varepsilon = 1/16$.

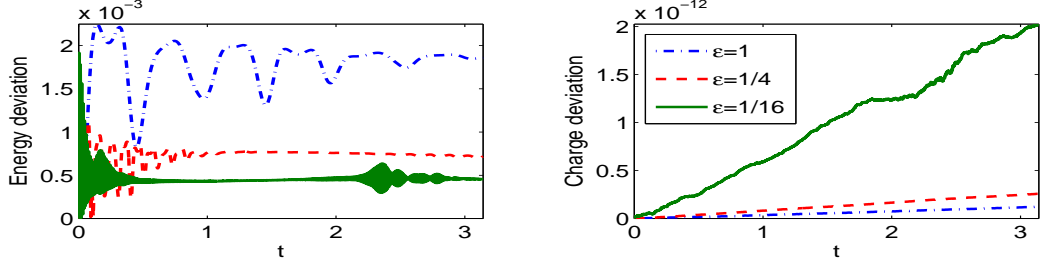


FIGURE 11. Deviation of the energy (1.5) and the charge (1.6) of the computation by MRC in Fig. 9: $|E^n - E(0)|/|E(0)|$ and $|Q^n - Q(0)|/|Q(0)|$.

the numerical energy is just a small fluctuation from the initial value and the charged is preserved to machine accuracy.

5. CONCLUSION

We considered the rotating nonlinear Klein-Gordon (RKG) equation which contains first order and second order angular momentum operator terms for modelling a rotating galaxy in cosmology. We showed that in the non-relativistic limit regime, RKG formally converges to a coupled rotating nonlinear Schrödinger (RNLS) model. In fact, the limit RNLS model describes the dynamics of the rotating two-component Bose-Einstein Condensates. We discussed and compared the RKG model with the RNLS. We then presented numerical algorithms for efficiently solving the RKG in polar coordinates or in Cartesian coordinates. In particular, we applied a rotating Lagrangian coordinates transform which eliminates both angular terms in the RKG, so that the multiscale strategies were further applied to get uniformly accurate numerical schemes for solving the RKG in the non-relativistic limit regime. With the proposed methods, we studied the quantized vortices dynamics in RKG from relativistic regime to the non-relativistic regime. Simulation results were presented in the end.

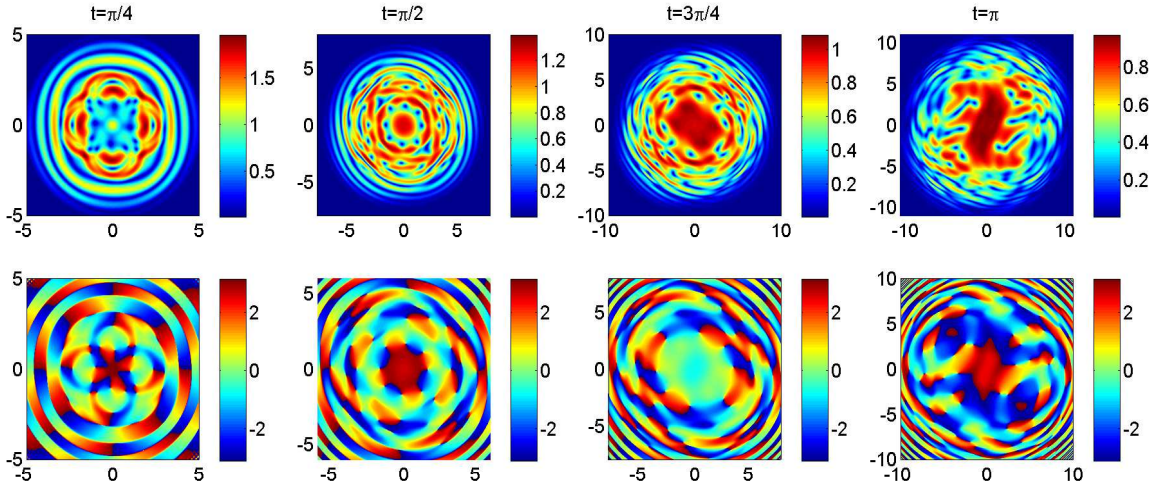


FIGURE 12. Contour plot of $|\Psi|$ and $\text{Arg}(\Psi)$ in example 4.3 with non-symmetric potential at different t under $\varepsilon = 1/4$.

ACKNOWLEDGEMENTS

The work is dedicated to the memory of Prof. Kerson Huang. X. Zhao is partially supported by the French ANR project MOONRISE ANR-14-CE23-0007-01, the Natural Science Foundation of Hubei Province No. 2019CFA007 and the NSFC 11901440. Y. Zhang was supported by the Austrian Science Foundation (FWF) via his Schrödinger Fellowship J3784-N32, and under grant No. F41 (SFB “VICOM”) and grant No. F65 (SFB “Complexity in PDEs”). Also support from the Wiener Wissenschafts und Technologiefonds (WWTF) project No. MA16-066 (“SEQUEX”) is acknowledged. We thank Dr. Chi Xiong for helpful discussions.

REFERENCES

- [1] P. ALLMER, N.J. MAUSER, Semiclassical limit of the Klein-Gordon equation, (2020) manuscript.
- [2] W. BAO, Y. CAI, Mathematical theory and numerical methods for Bose-Einstein condensation, Kinetic and Related Models 6 (2013) pp.1-135.
- [3] W. BAO, Y. CAI, X. ZHAO, A uniformly accurate multiscale time integrator pseudospectral method for the Klein-Gordon equation in the nonrelativistic limit regime, SIAM J. Numer. Anal. 52 (2014) pp.2488-2511.
- [4] W. BAO, X. DONG, Analysis and comparison of numerical methods for the Klein-Gordon equation in the non-relativistic limit regime, Numer. Math. 120 (2012) pp.189-229.
- [5] W. BAO, X. DONG, X. ZHAO, Uniformly accurate multiscale time integrators for highly oscillatory second order differential equations, J. Math. Study 47 (2014) pp.111-150.
- [6] W. BAO, Q. DU, Y. ZHANG, Dynamics of rotating Bose-Einstein condensates and its efficient and accurate numerical computation, SIAM J. Appl. Math. 66 (2006) pp.758-786.
- [7] W. BAO, H. LI, J. SHEN, A generalized-Laguerre-Fourier-Hermite pseudospectral method for computing the dynamics of rotating Bose-Einstein condensates, SIAM J. Sci. Comput. 31 (2009) pp.3685-3711.
- [8] W. BAO, D. MARAHRENS, Q. TANG, Y. ZHANG, A simple and efficient numerical method for computing the dynamics of rotating Bose-Einstein condensates via rotating Lagrangian coordinates, SIAM J. Sci. Comput. 35 (2013) pp.A2671-A2695.
- [9] W. BAO, Q. TANG, Numerical study of quantized vortex interaction in nonlinear Schrödinger equation on bounded domains, Multiscale Model. Simul. 12 (2014) pp.411-439.
- [10] W. BAO, Q. TANG, Numerical study of quantized vortex interaction in the Ginzburg-Landau equation on bounded domains, Commun. Comput. Phys. 14 (2013) pp.819-850.
- [11] W. BAO, H. WANG, P.A. MARKOWICH, Ground, symmetric and central vortex states in rotating Bose-Einstein condensates, Comm. Math. Sci. 3 (2005) pp. 57-88.
- [12] W. BAO, X. ZHAO, Comparison of numerical methods for the nonlinear Klein-Gordon equation in the nonrelativistic limit regime, J. Comput. Phys. 398 (2019) pp. 108886.
- [13] D.D. BAINOV, E. MINCHEV, Nonexistence of global solutions of the initial-boundary value problem for the nonlinear Klein-Gordon equation, J. Math. Phys. 36 (1995) pp.756-762.

- [14] W. BAO, R. ZENG, Y. ZHANG, Quantized vortex stability and interaction in the nonlinear wave equation, *Physica D* 237 (2008) pp.2391-2410
- [15] S. BAUMSTARK, E. FAOU, K. SCHRATZ, Uniformly accurate exponential-type integrators for Klein-Gordon equations with asymptotic convergence to the classical NLS splitting, *Math. Comp.* 87 (2018) pp.1227-1254.
- [16] P. BECHOUCHE, N.J. MAUSER, S. SELBERG, Nonrelativistic limit of Klein-Gordon Maxwell to Schrödinger-Poisson, *Amer. J. Math.* 126 (2004) pp.31-64.
- [17] V.B. BEZERRA, H.S. VIEIRA, A.A. COSTA, The Klein-Gordon equation in the spacetime of a charged and rotating black hole, *Class. Quantum Grav.* 31 (2014) pp.045003.
- [18] J.P. BOYD, F. YU, Comparing seven spectral methods for interpolation and for solving the Poisson equation in a disk: Zernike polynomials, Logan-Shepp ridge polynomials, Chebyshev-Fourier Series, cylindrical Robert functions, Bessel-Fourier expansions, square-to-disk conformal mapping and radial basis functions, *J. Comput. Phys.* 230 (2011) pp. 1408-1438.
- [19] J.D. BJORKEN, S. DRELL, *Relativistic Quantum Fields*, McGraw-Hill (1965).
- [20] PH. CHARTIER, N. CROUSEILLES, M. LEMOU, F. MÉHATS, Uniformly accurate numerical schemes for highly oscillatory Klein-Gordon and nonlinear Schrödinger equations, *Numer. Math.* 129 (2015) pp.211-250.
- [21] PH. CHARTIER, N. CROUSEILLES, X. ZHAO, Numerical methods for the two-dimensional Vlasov-Poisson equation in the finite Larmor radius approximation regime, *J. Comput. Phys.* 375 (2018) pp.619-640.
- [22] PH. CHARTIER, J. MAKAZAGA, A. MURUA, G. VILMART, Multi-revolution composition methods for highly oscillatory differential equations, *Numer. Math.* 128 (2014) pp.167-192.
- [23] PH. CHARTIER, F. MÉHATS, M. THALHAMMER, Y. ZHANG, Convergence analysis of multi-revolution composition time-splitting pseudo-spectral methods for highly oscillatory differential equations of Schrödinger equations, *ESAIM:M2AN* 51 (2017) pp.1859-1882.
- [24] S.K. CHAKRABARTI, P.R. GIRI, K.S. GUPTA, Normal mode analysis for scalar fields in BTZ black hole background, *Eur. Phys. J C* 60 (2009) pp.169-173.
- [25] X. DONG, Z. XU, X. ZHAO, On time-splitting pseudospectral discretization for nonlinear Klein-Gordon equation in nonrelativistic limit regime, *Commun. Comput. Phys.* 16 (2014) pp.440-466.
- [26] S. DETWEILER, Klein-Gordon equation and rotating black holes, *Phys. Rev. D* 22 (1980) pp.2323.
- [27] E. FAOU, K. SCHRATZ, Asymptotic preserving schemes for the Klein-Gordon equation in the non-relativistic limit regime, *Numer. Math.* 126 (2014) pp.441-469.
- [28] H.R.C. FERREIRA, C.A.R. HERDEIRO, Stationary scalar clouds around a BTZ black hole, *Phys. Lett. B* 773 (2017) pp.129-134.
- [29] V.L. GINZBURG, L.D. LANDAU, Toward the superconductivity theory, *Zh. Eksp. Teor. Fiz.* 20 (1950) pp. 1064.
- [30] M. GOOD, C. XIONG, A. CHUA, K. HUANG, Geometric creation of quantum vorticity, *New J. Phys.* 18 (2016) pp.113018.
- [31] Y. GUO, X. LIU, C. XIONG, X. XU, C. FU, Towards high-quality visualization of superfluid vortices, *IEEE Trans. Vis. Comput. Graph.* 24 (2018) pp. 2440-2455.
- [32] E. HAIRER, CH. LUBICH, G. WANNER, *Geometric Numerical Integration: Structure-Preserving Algorithms for Ordinary Differential Equations*, Springer, Berlin, 2006.
- [33] D.S. HALL, M.R. MATTHEWS, J.R. ENSHER, C.E. WIEMAN, E.A. CORNELL, Dynamics of component separation in a binary mixture of Bose-Einstein condensates, *Phys. Rev. Lett.* 81 (1998) pp.1539-1542.
- [34] T.L. HO, V.B. SHENOY, Binary mixtures of Bose condensates of alkali atoms, *Phys. Rev. Lett.* 77 (1996) pp.327-3279.
- [35] M. HOCHBRUCK, A. OSTERMANN, Exponential integrators, *Acta Numer.*, 19 (2010) pp. 209-286.
- [36] K. HUANG, *A Superfluid Universe*, World Scientific, 2016. (ISBN 9813148454).
- [37] K. HUANG, C. XIONG, X. ZHAO, Scalar-field theory of dark matter, *Internat. J. Modern Phys. A* 29 (2013) pp.1450074.
- [38] K. HUANG, H. LOW, R. TUNG, Scalar Field Cosmology II: Superfluidity, Quantum Turbulence, and Inflation, *Internat. J. Modern Phys. A* 27 (2012) pp.1250154.
- [39] D.G. LEVKOV, A.G. PANIN, I.I. TKACHEV, Gravitational Bose-Einstein condensation in the kinetic regime, *Phys. Rev. Lett.* 121 (2018) pp.151301.
- [40] B. LI, Z. ZHANG, A new approach for numerical simulation of the time-dependent Ginzburg-Landau equations, *J. Comput. Phys.* 303 (2015) pp. 238-250.
- [41] J. JIN, S. ZHANG, W. HAN, Z. WEI, The ground states and spin textures of rotating two-component Bose-Einstein condensates in an annular trap, *J. Phys. B: At. Mol. Opt. Phys.* 46 (2013) pp.075302.
- [42] K. KASAMATSU, M. TSUBOTA, M. UEDA, Vortex phase diagram in rotating two-component Bose-Einstein condensates, *Phys. Rev. Lett.* 91 (2003) pp.150406.
- [43] A.K. KASSAM, L.N. TREFETHEN, Fourth-order time-stepping for stiff PDEs, *SIAM J. Sci. Comput.* 26 (2005) pp. 1214-1233.
- [44] I.M. KHALATNIKOV, *An Introduction to the Theory of Superfluidity*, Addison-Wesley, New York, 1989.
- [45] M.C. LAI, W.W. LIN, W. WANG, A fast spectral/difference method without pole conditions for Poisson-type equations in cylindrical and spherical geometries, *IMA J. Numer. Anal.* 22 (2002) pp.537-548.
- [46] H.B. LOW, C. XIONG, *Fantasia of a Superfluid Universe-In Memory of Kerson Huang*, arXiv:1612.01347.
- [47] N.J. MAUSER, Y. ZHANG, Exact artificial boundary condition for the Poisson equation in the simulation of the 2D Schrödinger-Poisson system, *Commun. Comput. Phys.* 16 (2014) pp.764-780.

- [48] J. MING, Q. TANG, Y. ZHANG, An efficient spectral method for computing dynamics of rotating two-component Bose-Einstein condensates via coordinate transformation, *J. Comput. Phys.* 258 (2014) pp.538-554.
- [49] S. MACHIHARA, K. NAKANISHI, T. OZAWA, Nonrelativistic limit in the energy space for nonlinear Klein-Gordon equations, *Math. Ann.* 322 (2002) pp.603-621.
- [50] N. MASMOUDI, K. NAKANISHI, From nonlinear Klein-Gordon equation to a system of coupled nonlinear Schrödinger equations, *Math. Ann.* 324 (2002) pp.359-389.
- [51] N.J. MAUSER, Semi-relativistic approximations of the Dirac equation: first and second order corrections, *Transp. Theor. Stat. Phys.* 29 (2000) pp.122-137.
- [52] N.J. MAUSER, S. SELBERG, Convergence of the Dirac-Maxwell system to the Vlasov-Poisson system, *Comm. PDE* 32 (3) (2007) pp.503-524
- [53] C.J. MYATT, E.A. BURT, R.W. GHRIST, E.A. CORNELL, G. E. WIEMAN, Production of two overlapping Bose-Einstein condensates by sympathetic cooling, *Phys. Rev. Lett.* 78 (1997) pp. 586-589.
- [54] B. NAJMAN, The nonrelativistic limit of the nonlinear Klein-Gordon equation, *Nonlinear Anal.* 15 (1990) pp.217-228.
- [55] B. POURHASSAN, The Klein-Gordon equation of a rotating charged hairy black hole in (2+1) dimensions, *Modern Phys. Lett. A* 31 (2016) pp.1650057.
- [56] D.J. ROWAN, G. STEPHENSON, The Klein-Gordon equation in a Kerr-Newman background space, *J. Phys. A: Math. Gen.* 10 (1977) pp.15-23.
- [57] J. SHEN, T. TANG, L. WANG, *Spectral Methods: Algorithms, Analysis and Applications*, Springer, 2011.
- [58] Q. TANG, Y. ZHANG, N.J. MAUSER, A robust and efficient numerical method to compute the dynamics of the rotating two-component dipolar Bose-Einstein condensates, *Comput. Phys. Comm.* 219 (2017) pp.223-235.
- [59] L. TREFETHEN, *Spectral Methods in Matlab*, Oxford University, Oxford, 2000.
- [60] M. TSUBOTA, K. KASAMATSU, M. UEDA, Vortex lattice formation in a rotating Bose-Einstein condensate, *Phys. Rev. A* 65 (2002) pp. 023603.
- [61] P. VALTANCOLI, Scalar field conformally coupled to a charged BTZ black hole, *Ann. Physics* 369 (2016) pp. 161-167.
- [62] C. XIONG, M. GOOD, Y. GUO, X. LIU, K. HUANG, Relativistic superfluidity and vorticity from the nonlinear Klein-Gordon equation, *Phys. Rev. D* 90 (2014) pp.125019.
- [63] C. XIONG, K. HUANG, Relativistic two-fluid hydrodynamics with quantized vorticity from the nonlinear Klein-Gordon equation, *arXiv:1612.09248*.
- [64] O. WALDRON, R. A.VAN GORDER, A nonlinear Klein-Gordon equation for relativistic superfluidity, *Phys. Scripta* 92 (2017), pp.105001.
- [65] , Y. WANG, X. ZHAO, Symmetric high order Gautschi-type exponential wave integrators pseudospectral method for the nonlinear Klein-Gordon equation in the nonrelativistic limit regime, *Int. J. Numer. Anal. Model.* 15 (2018), pp. 405-427.
- [66] S. WEINBERG, *The Quantum Theory of Fields, Volume 1: Foundations*. Cambridge University Press, 1995.
- [67] E. WITTEN, Superconducting strings, *Nucl. Phys. B* 249 (1985), pp.557-592.
- [68] W.H. ZUREK, Cosmological experiments in superfluid helium? *Nature* 317 (1985) pp.505-508.
- [69] Y. ZHANG, W. BAO AND H. LI, Dynamics of rotating two-component Bose-Einstein condensates and its efficient computation, *Phys. D* 234 (2007) pp.49-69.

N. MAUSER: WOLFGANG PAULI INSTITUTE C/O FAK. MATHEMATIK, UNIV. WIEN, OSKAR-MORGENSTERN-PLATZ 1, A-1090, VIENNA.

E-mail address: norbert.mauser@univie.ac.at

URL: <https://www.wpi.ac.at/director.html>

Y. ZHANG: CENTER FOR APPLIED MATHEMATICS, TIANJIN UNIVERSITY, TIANJIN 300072, CHINA

E-mail address: Zhang.Yong@tju.edu.cn

URL: <http://cam.tju.edu.cn/~yzhang/>

X. ZHAO: SCHOOL OF MATHEMATICS AND STATISTICS, WUHAN UNIVERSITY, 430072 WUHAN, CHINA; UNIV. RENNES, INRIA-MINGUS, CNRS, IRMAR-UMR 6625, F-35000 RENNES, FRANCE

E-mail address: matzhxf@whu.edu.cn

URL: <http://jszy.whu.edu.cn/zhaoxiaofei/en/index.htm>